

## Response to Reviewer Comments for:

### “Basal traction mainly dictated by hard-bed physics over grounded regions of Greenland”

#### Comments from Bradley Lipovsky (Referee)

**Comment:** Dear Maier and coauthors,

I am happy to have been asked to review this paper. Its topic and methods are at the cutting edge and the results will be interesting to readers of the Cryosphere. I'd like to highlight several ways that the paper could be improved.

Sincerely,

Brad Lipovsky

**Response:** Thank you for taking the time to review the manuscript and making very constructive comments.

**Comment:** 1. Length scale for grid cells. I like the approach in Section 2.4 but I think it could be made better: My main concern is that Figure 2 compares different regions with different force balance approximations. Wouldn't it be better to compare the \*same\* regions with different force balance approximations? In other words, to carry out a grid-refinement study, and then examine the convergence behavior of different force balance approximations? -I would expect the relevant length scale for SIA-SSA differences to be quite high in the interior (far greater than 6km) but much smaller near the margins (perhaps even less than 6km). - Figure 2 could be on a log scale so we can see if there is a change in the power law. The 6km cutoff seems arbitrary. I don't see anything special about 6km in Figure 2. Again, if you plot this on log-log axes I have a feeling it will make a straight line (i.e., a power law) with nothing special about the 6km cutoff.

**Response:** Thank you for the detailed comment. We are assuming this comment addresses Section 2.3 rather than 2.4 since it is the section addressing length scales. We shall clarify first that in the analysis presented in Figure 2 the mean difference between the data SIA and SSA data  $\underline{\delta}$  derived from directly comparing the traction for the same grid cells across the ice sheet (Fig. 2) which is outlined in Section 2.3. However, as you highlight, our length-scale justification is a compromise between the ideal physically based choice and more practical considerations. In the ideal case, the length scale would be optimized when the difference between the SIA and SSA no longer decreases moving up to a coarser grid cell implying the influence of stress gradients are perfectly minimized. However, our length scale choice also considers several other criteria that we decide are needed to fit the requirements of our study. Specifically, we take into consideration the resolution near edges of the ice sheet and the span of the velocity range used to derive the relationships. Each of these requirements favor shorter length scales. In the end, we settle on 6km because it minimizes the difference between the SSA and SIA reasonably well (Figure. 2), and it maximizes the resolution and inclusion of grid cells near the margin as well as the velocity range. Most importantly we show that moving up to a larger grid cell does not change our interpretation. This rational for this decision is outlined in lines 159-163 in the main text of the original manuscript.

In terms of the technical aspects of the length scale optimization, the reviewer correctly points out that the longitudinal coupling length scale varies with ice thickness. Thus, the ideal length scale where stress gradients are minimized would vary across the ice sheet and would be significantly different for thick and thin ice. To simplify our analysis, we assume that at the chosen length scale stress gradients are minimized reasonably well everywhere. This includes the thinner margin regions where ice flow is more complex, as well as the thick interior where flow varies smoothly and slowly in space. To show that the 6 km length scale is a reasonable choice across a wide range of ice thicknesses and settings, we separate the data set into thick and thin ice (below and above 1500 m ice thickness), and inland and interior regions (below and above 1200 m.a.s.l.) to see how much the difference between the SIA and SSA changes. We find at 6 km there only a small change (0.004 MPa) in the difference between the SSA and SIA between the four different data subsets (Figure R1). While it may seem counter intuitive for the difference to be less for the interior grid cells where the longitudinal coupling distance ( $\sim 10 \times$  ice thickness) are expected to be greater, ice flow is generally much less complex than near the margins, and thus magnitude of the stress gradients in general are likely lower.

We also address the reviewer suggestion of having Figure 2 of main text shown in log-log (Figure R2). In log space the optimization does not show true power law behavior and still has curvature. We feel that for the linear scale plot is more intuitive for the reader and keep the linear scale plot in the main text.

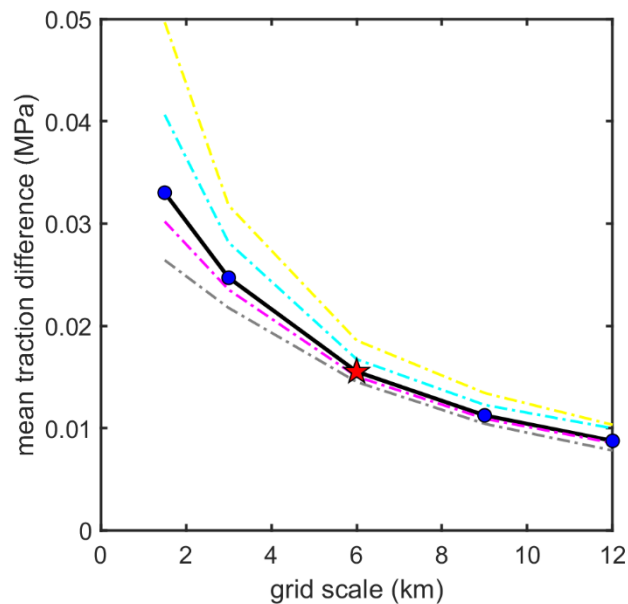


**Figure R1:** Mean traction difference (magnitude of SIA minus SSA) between the SIA and SSA approximation of basal traction as a function of grid scale. Decreasing deviation indicates the effect of higher-order stresses decreases with increasing grid length. Red star shows 6 km grid scale which is the primary grid scale used for our analysis. Dashed lines show same analysis for different subsets of the data (margin regions < 1200 m.a.s.l. – yellow line, interior regions > 1200 m.a.s.l. – grey line, thickness > 1500 m – magenta line, thickness < 1500 m – cyan line).

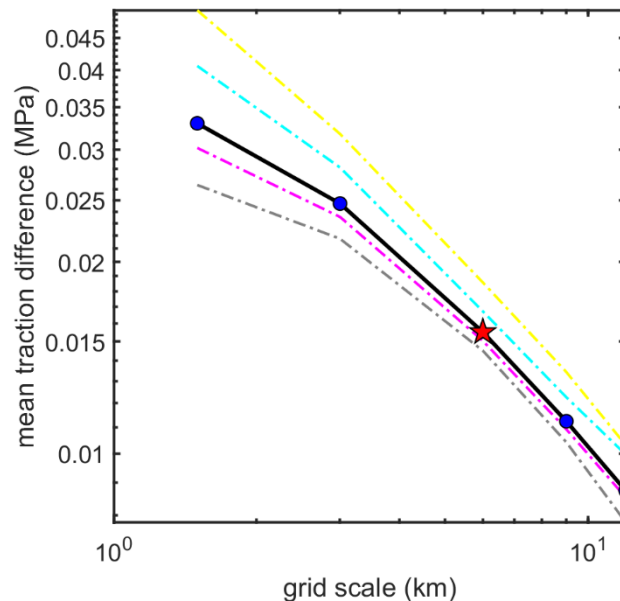


**Figure R2:** Same figure as above but in log space. Mean traction difference (magnitude of SIA minus SSA) between the SIA and SSA approximation of basal traction as a function of grid scale. Decreasing deviation indicates the effect of higher-order stresses decreases with increasing grid length. Red star shows 6 km grid scale which is the primary grid scale used for our analysis. Dashed lines show same analysis for different subsets of the data (margin regions < 1200 m.a.s.l – yellow line, interior regions > 1200 m.a.s.l – grey line, thickness > 1500 m – magenta line, thickness < 1500 m – cyan line).

**Comment:** 2. How well resolved is the sliding law at high velocity? Of course there are many fewer data points in this regime because most of the ice sheet is slow-flowing. One idea is that, in Figure 5, plotting PDFs rather than CDFs would more accurately convey to the reader that there are very few data points at high velocity. This is an important point to convey. Concerning Catchment 2, the increase in basal traction at high velocities is very strange. I'm worried that this increase is based on only a very small number of data points (CDF is almost flat at high velocities). Question: Is there some way that you could re-draw Figures 5 to \*combine\* the CDF and velocity/traction curve? Example: what if the opacity of the curve was set by the number of observations? Drawing the curves in this way would highlight the areas that are more well captured by the data. This is just a guess about how to convey this point. . . no worries if it doesn't work out.

**Response:** While we give equal weighting to the high and low velocity regions through median binning, some of the bins have much less data, and as you point out, there is less certainty in the central tendency at high velocities. However, since each relationship is catchment specific, the median of the high velocity bins still does reflect the data in the catchment. To make it clear that there is less data at high velocities, we add a PDF as the reviewer suggested in Fig 5. We also tried different variants of the opacity idea you proposed, but found it makes the figure a more confusing.

Concerning catchment 2, we do find increasing traction at high velocities which indicates that in fastest flowing regions of this catchment we likely have grid cells that are probably more consistent with rate

strengthening. The traction relationships (bins, fits, etc.) presented in the manuscript are for large areas where spatially varying bed properties are likely. Accordingly, the traction relationships are meant to be interpreted in terms of the predominant physics that would produce the main features relationship in each catchment (i.e. rate strengthening or Mohr-Coulomb-like behavior), rather than taken at face value. As you point out, we have some catchments that show “mixed” behavior, and thus our relationships do not perfectly match the idealized traction relationships presented in Figure 3. However, in the case of catchment 2, there are very few data points that show high velocities and high tractions, and thus the bulk catchment behavior is best characterized as Mohr-Coulomb-like as outline in Section 4.2.2. To help clear up any confusion on how we draw conclusions on the predominate behavior in each catchment, we added additional text at the beginning of section 4.2 (lines 355-357).

**Comment:** 3. Many catchments show rate strengthening at high velocities, a non-intuitive result for me. Based on Figure 3, I would have thought that these velocities were high enough to reach rate-weakening behavior. From Gagliardini’s paper, Equation 24, we may therefore place bounds on subglacial parameters. It would be interesting to see if you could constrain  $A$  or  $C$  from your observations.

**Response:** The adherence to rate strengthening for ice speeds near 1000 m/yr in some catchments was surprising for us as well and interestingly demonstrates in catchments 3 and 4 of the ice sheet, very high velocities can simply arise from high stress. This also implies that  $CN$  for these catchments is also high (discussed further below). Figure 3 was not meant for quantitative comparison, but instead was meant to be demonstrative of the qualitative features that can be used to distinguish the three basic types of traction relationships (i.e. the kink and increased curvature expected for deforming beds and hard beds with cavitation). As such, the value of  $CN$  which sets Iken’s bound for the Gagliardini curve (black curve, Fig. 3) is set arbitrarily to fit the bound in the plotting space. We clarify this in the figure caption to avoid further confusion.

Constraining physical parameters using our traction relationships is definitely a logical idea. However, we hesitate to do so in all cases because depending on the parameter of interest, differing degrees of assumptions and simplifications are needed. The big distinction between our relationships and sliding relationships is that the ice motion used to derive them includes deformation which would influence some of the hard bed sliding parameters if calculated directly from the relationship. As per the traction law presented in Gagliardini et al., 2007 (also defined as Eq. 3 in our paper),  $C$  is not independent from  $N$ . Yet  $CN$  can still be constrained as a lumped parameter. Since  $CN$  is a stress it can be confidently inferred using a flow relationship that includes deformation. We provide a lower bound on  $CN$  for Catchment 3 and 4 which are the catchments that clearly show rate strengthening through the entire velocity range for all the inversions indicating hard- bed behavior is likely. We add text to section 4.2.1. to explicitly quantify this in the manuscript (Lines 371-374).

In the Mohr-Coulomb-like catchments we find increases in curvature at high velocities which could be consistent with either Iken’s bound  $CN$  or the till strength,  $\tau_*$ . (Fig. 3-5). We add text to section 4.2.2. to explicitly quantify this in the manuscript (Lines 405-407).

$A_s$  can be also constrained using the traction law given in Gagliardini et al. 2007 from the rate parameter  $C_p$  and exponent  $p$  of Eq. 3 by assuming bed shape parameter  $q = 1$ ,  $p = n$  ( $n$  is the nonlinear flow exponent of ice),  $CN$  is large, and the surface velocity is roughly equivalent to the sliding velocity. In this case the relationship will collapse back into a Weertman relationship and thus can be approximated using

*Eq. 2.* Given these assumptions we find  $A_s = 1.1 \cdot 10^6$  and  $4.4 \cdot 10^5 \text{m yr}^{-1} \text{MPa}^{-m}$  for the SSA and SIA respectively in catchment 3, and  $A_s = 3.2 \cdot 10^6$  and  $6.7 \cdot 10^5 \text{m yr}^{-1} \text{MPa}^{-m}$  in catchment 4. The large range reflects high sensitivity to small differences in  $m$  found in the different inversions. Given the uncertainty in  $m$  (presented in Table S1), the assumptions needed to simplify the traction relationship ( $q$  is unlikely to equal 1), and importantly that  $C_p$  was derived using surface velocities, we choose not to constrain the sliding parameter  $A_s$  in the manuscript.

## **Comments from Anonymous Referee #2**

**Comment:** This is a well-written manuscript that reflects a lot of hard work by the authors. It sets up an interesting and thoughtful experiment, assessing basal traction with three different model hierarchies.

**Response:** Thank you for taking the time to review it and providing us with thoughtful and constructive criticism.

**Comment:** Main Concerns:

- A large basis of the conclusion relies on the relationships in the scatter plots in Figure 4. These are on a log-log scale and even then the scatter is so great that I am skeptical any credible conclusion can be drawn from these graphs. Binning the velocities and taking the median, especially in log-log space looks better, but does seem kind of sneaky. I am particularly nervous about the unequal distribution of velocities, since fewer data points exist in the faster flowing regions in making the bins. So, while ‘fitting the binned data gives equal weights to fast flowing and slow flowing regions of each catchment’ (line 247), many of the faster flowing bins only have a handful of data points, so the fit is biased by the slower regions.

I am sympathetic that these ‘tricks’ are needed in order to get the clean-looking relationships that are distilled in Figure 5. However, Figure 4 really highlights the incredible complexity of this relationship that gets glossed over in the subsequent discussion and conclusions. Instead, every kink in the fitted curve is analyzed in great detail. Figure 8, which shows a map of strong vs weak bed grid cells, takes this (in my opinion) messy relationship and derives some binary conclusions about the preponderance of hard-bedded rheology. At 6 km data points, then binned to derive the traction-velocity relationship, the impact of the fastest flowing regions is muted.

**Response:** We really appreciate the core of this criticism. The challenge of working with big data sets is distilling the data into something meaningful while still properly acknowledging the variability and limitations which is what we are striving to achieve in the manuscript. However, we strongly feel conclusions can be drawn from the data and analysis, and further, that those presented in the manuscript are well supported. The current state of knowledge in Greenland is that there is no relationship between velocity and traction for the fast-flowing marine terminating glaciers as found by Stearns et al. 2018, and it is unclear whether those findings apply further inland and in regions without marine-terminating glaciers. Our analysis is designed to fill this knowledge gap, and further, does it in a novel way that minimizes the biases associated with unconstrained model parameters to generate velocity-traction relationships that can be confidently interpreted in terms of bed physics.

The reviewer correctly points out, there is scatter in the relationships even after averaging the traction and velocity over large grid cells. This is expected given the variety of different substrate, bed properties, and hydrologic conditions that are likely to exist under Greenland. Yet, even in the raw data, we can simply look at distribution of grid cells in catchments 3-4 and 6-8 and visually see that tractions increase with velocity. At high velocities, tractions are also high, and there are very few grid cells that could be characterized otherwise in either the log scale or linear scale plots (Figure R3) presented below. Thus, to a first-order, and just from the raw data, we can already determine that there is a basic rate-strengthening relationship which is consistent with theoretical expectations for ice flow over hard beds and contrasts with the work of Stearns et al. 2018 which focused on marine terminating glaciers and found no relationship between the variables.

Binning the data through the velocity range by calculating the median IQR, and 90% of the detail allows us to take the analysis further by statistically determining the finer details of the traction relationship through the velocity range. Binning is a commonly used statistical approach in our field (Armstrong et al., 2017; Dehecq et al., 2019; Stevens et al., 2018) and for large data sets in general. We find that the catchments where rate strengthening was identifiable in the raw data again clearly show rate strengthening in the binned data. The small spread of the IQR indicates the bins well represent a large portion of the data giving us confidence that the binned relationships are representative of physical conditions across a large fraction of most catchments. Similarly, the binned statistics also show where there is more complexity. For instance, while the binned data show good adherence to rate strengthening in catchment 6, the IQR and 90<sup>th</sup> percentile indicate Mohr-coulomb-behavior. Using these statistical attributes and the high quantity of weak-bed grid cells allows us to make the more nuanced interpretation that grid cells in this catchment can reflect either rate strengthening and Mohr-Coulomb-like behavior and thus the bed rheology is best classified as mixed.

The data binning also allows us to identify important structure in the predominantly Mohr-Coulomb-like catchments (1 and 2). For example and as the reviewer points out, the raw data in catchment 2 has a large degree of scatter with no obviously discernable structure. However, once binned, we can see that there is rate strengthening with a sharp break in slope moving to higher velocities, which is consistent with Mohr-Coulomb like behavior. Thus, we can infer that the increased scatter likely reflects the velocity independence of Mohr-Coulomb physics, allowing us to make a more precise interpretation beyond that there isn't a relationship between the variables from looking at the raw data.

We do not feel that our interpretations and conclusions are binary. The interpretations in section 2.4 acknowledge the data variability and are robust in the sense that they rely on several different aspects of the data; model fits, characteristics of the binned relationship, distribution of grid cells, data scatter, differences in the inversions, and catchment-specific preexisting knowledge. They also identify uncertainty using the spread in the SIA, SSA, and FS, as well as the binned statistics. Further, the paper is filled with qualifiers (*section headings for 2.4.1 - 2.4.4*) and nuance (*Section 4.3*) which were purposefully put in to indicate we are not drawing sharp binary conclusions from the dataset. However, we feel our results and analysis well support our mainly conclusion which is summarized in the manuscript title "Hard-bed physics mainly dictates basal traction over grounded regions of Greenland". We are not claiming hard-bed physics applies everywhere, but except for the NEGIS and some tidewater glaciers, we mostly find behavior consistent with rate strengthening. This is an import "fuzzy constraint" which can be useful for ice sheet modelers and hopefully serve as a starting point for future investigations that look at bed properties across smaller spatial scales. However, to address this comment in general, we changed the text in several locations throughout the manuscript where our language was too definitive (highlighted in yellow, lines 17, 426, 472, 482, 512). We also added text to the conclusions to make clear that our findings reflect the relationships where the velocity and traction are averaged over large scales. This serves as an important starting point for future work to look at location specific bed properties and traction laws across finer scales (Lines 514-516).

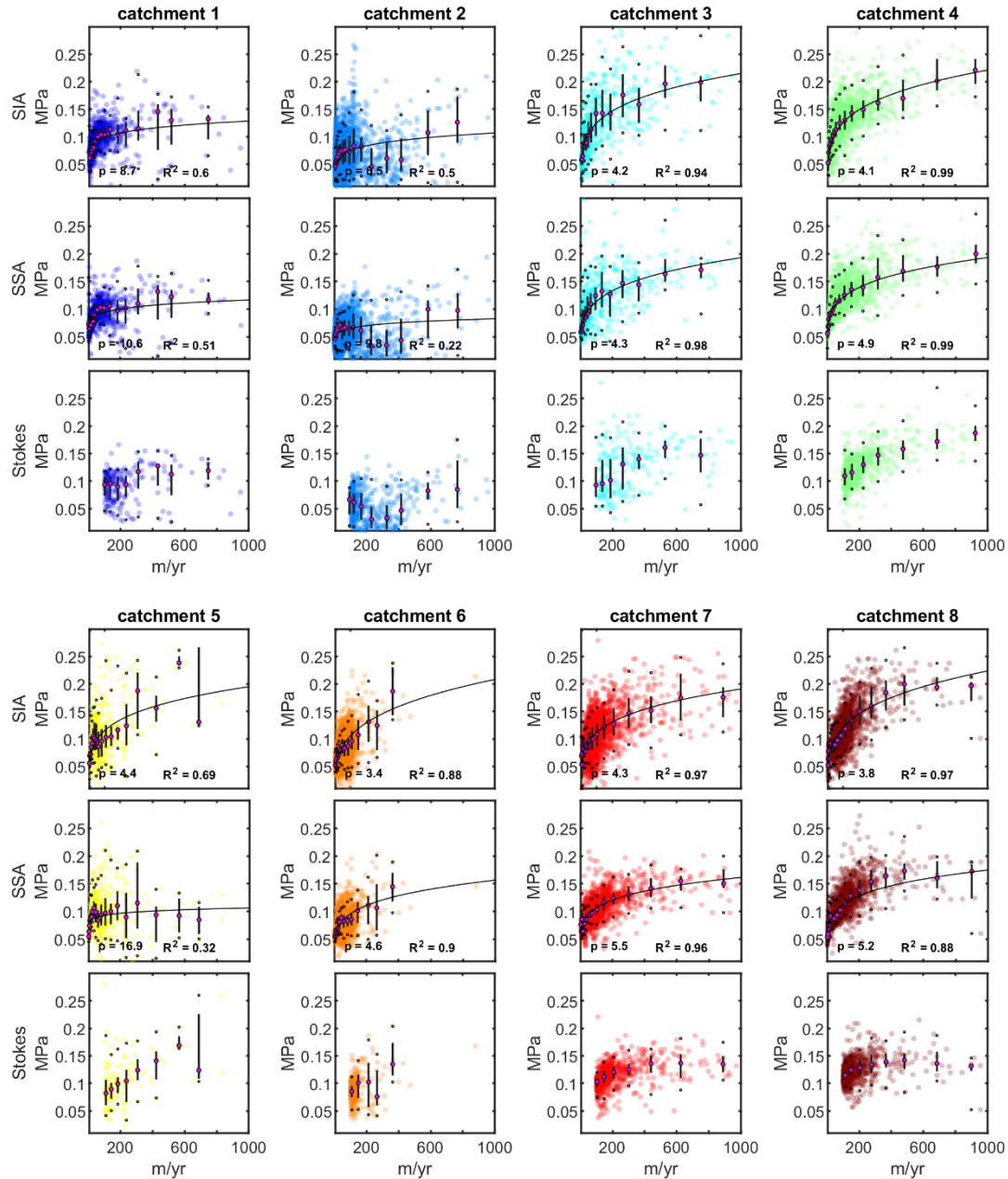


**Figure R3:** Same as Figure 4 in the main text except on a linear scale. The velocity – traction relationship for the SIA, SSA, and Full Stokes inversions for all eight drainage catchments. Transparency is an indicator of data density, where opaque areas indicate four or more grid cells occupy the same marker area on the plot. Magenta markers show the median traction values for 20 logarithmically spaced velocity bins, the vertical bars show the interquartile range, and the black dots indicate the middle 90 percent of the data. Black line shows a power law model fit to the binned data. No models were fit to the stokes relationships due to the velocity range ( $> 100$  m/yr) which is limited in our analysis.

**Comment:** - The assumption (section 2.2.1) that basal drag can be approximated by the driving stress works for the interior but really falls apart near the margins. As a result, I think the limit of this analysis precludes a lot of the faster flowing regions. Given that shortcoming, the overall conclusions are weaker.

**Response:** The strength of using three different traction inversions is it allows us to infer where the driving stress may not be a good approximation for the traction. The applicability of the driving stress depends on the complexity of the flow field and the basal topography, and thus, this approximation does not necessarily fall apart near the margins. We find close correspondence between the SIA, SSA, and FS solutions up to relatively high velocities ( $\sim 300$  m/yr) in most catchments 5-8 and at even higher velocities in catchments 3-4, suggesting the SIA is a reasonable approximation at relatively high velocities. However, the hierarchical approach does highlight velocities where there are large differences between the inversions where the driving stress might not be a good approximation for the traction. This divergence is most prominent in the higher velocity zones of catchment 7 and 8. Our conclusions and interpretations of these catchments (*section 2.4.1*) account for this uncertainty.

- While it is done frequently, it is incredibly circular to prescribe a sliding relation to estimate basal drag and then use the calculated basal drag to show a correlation with velocity (*section 2.2.2 and 2.2.3*). The whole justification for this is described in line 137: While a linear sliding law is used for the inversion, the traction field is shown to have little sensitivity to the choice of sliding law (Joughin et al., 2004)." This paper uses the control method exclusively for the Ross Ice Streams (no basal drag and high velocity), which is opposite to how it's being used here.

**Response** Thank you for your comment. A choice of sliding law is necessary to numerically relate the traction and velocity to solve the force balance at each location for the SSA and FS inversions. We can see how it would seem mathematically circular to do so. Below we explain why that is not the case, and further why our large-scale averaging diminishes the role of any model – specific parameters.

Using the control method, the basal shear stress is estimated to maintain the stress equilibrium at each location and converges on the same value regardless of the form of the sliding relationship applied. The only assumption is that basal drag and sliding velocity are co-linear and thus can be related by a free parameter  $\beta$ . The inversion leads to spatial fields that allow a close match with the velocity observations while maintaining the force balance. Since both velocity and traction are both solutions of the inversion the logic is not circular. (Joughin et al., 2004) demonstrated this for a synthetic case: "While we have described three parameterizations for  $\tau_b$  (viscous, plastic, vector plastic), inversion with any of these parameterizations proceeds roughly in the same manner and yields the basal shear stress that provides a force balance consistent with the model given by [equation \(1\)](#). Force balance is achieved regardless of the assumed bed rheology. As a result, even though [equation \(3\)](#) applies to a viscous bed,  $\beta^2$  is a free parameter, so force balance can be achieved even if the bed exhibits weak plastic rather than linear viscous behavior." This applies whether there is a Coulomb or Weertman-type glacier bed thus the glaciologic setting does not affect the derived velocity - traction relationships. The velocity – traction relationships we present in the paper demonstrate this. We find both Coulomb and Weertman-style non-linear velocity-traction relationships using a linear sliding relation to invert for the traction field.

Even though the traction solution is constrained by the momentum balance, at fine spatial resolution (approximately ice thickness and below) choice of sliding law combined with the choice of regularization (which dictates how smooth the solution should be) can produce some small-scale differences in the traction pattern (Habermann et al., 2013). However, since we are averaging over large grid cells these parameter choices have a minimal effect on the traction pattern since the basal traction is almost entirely balancing the gravitational stress.

Other comments:

**Comment:** Line 10: “three different methods” but with the same assumptions and workflow. It would be clearer to say models with three different levels of complexity. This comes up again in line 83ish. Having three models that are based on the same assumptions converge does not necessarily yield confidence in the velocity-traction relationship – just highlights where the complexity is unimportant.

**Response:** Thank you for the comment. We agree with the reviewer, a hierarchy with different complexity is an excellent way to frame the manuscript and it will be adopted in the introduction of the revised manuscript (lines 77-79). To clarify, only the SSA and FS are derived using similar methods. The SIA is calculated independently and directly from the data as per section 2.2.1. Further, with the large grid cells used in our analysis the ice the traction predominantly balances the gravitational driving stress at each grid cell. Since the gravitational stress is set by the geometry of the ice sheet there is no reason the tractions are likely to be biased where all three inversions converge. However, the assumptions on the momentum balance are quite different for the SIA, SSA, and FS and thus, the differences between the velocity – traction relationships can be assumed related to those assumptions.

**Comment:** Line 46: “bypassing” is too strong a word. We have some models that can be used to infer basal processes, but they are really far from capturing details from localized observations at the ice bed interface.

**Response:** Ok, we agree and have changed the text to. “Improvements over the last decade in satellite observations of surface velocity and geometry have made it possible to infer bed properties across ice thickness length scales based on ice dynamics (Gillet-Chaulet et al., 2016; Habermann et al., 2013; Minchew et al., 2016).” (Lines 44-45)

**Comment:** Line 76: How can rheology have impacted the findings of Stearns and van der Veen? This is a fairly bold statement; if you keep it in it needs justification. I think it’s ok to say it’s still under debate and leave it there.

**Response:** We agree and have removed the comment on rheology and made the change as suggested (see lines 73-75).

**Comment:** Line 254: What is meant by “visually well defined” and “show good agreement with the model fit at both high and low velocities”. I thought the model was fit to these binned points.

**Response:** The reviewer is correct the model is fit to the binned data. We are simply pointing out that relationship in the binned data is clear, and that fitting a power-law to these bins provides a reasonable fit. Since the following comment address the same section, the revised text is presented together in the next response.

**Comment:** Line 255: High R2 (.22 -.99)? It’s more representative to specify where it’s high and where it isn’t - especially since it’s closer to .99 in most places. Also specify what the R2 value refers to (binned or raw data).

**Response:** This is a good idea and ties into our interpretations in section 4.2 (lines 258-263). We will change the description of the R<sup>2</sup> text to make it more specific as follows:

“The relationship between the binned variables (magenta dots) is visually well defined in all catchments and for each estimate of traction. In general, there is good agreement with the binned data and model fit at both high and low velocities. The R<sup>2</sup> is high in catchments 3, 4, and 6 through 8 [0.88 – 0.99] indicating

that the power-law model generally describes most of the variability of the binned relationships (Figure 4, supporting Table S1) for the SIA and SSA tractions. In the remaining catchments (1, 2, and 5) the  $R^2$  is lower [0.22 – 0.69], which results from the increasing curvature in the binned data at higher velocities which is not captured with the power law..”

Figure 5: Add labels of catchment to each subplot for color-blind folks. Is the grey line the cdf of the binned velocity data or the input data? I’m guessing the latter, which is misleading because the velocity-traction curves are based on the binned data. Don’t these graphs also show that the models diverge at fast flow (I didn’t like framing the models this way at the start, but since you did it tshould be revisited).

**Response:** The reviewer is correct that the CDF is for the actual data distribution and not the binned data. This was a mistake on our part which we correct on the updated figure. We also add PDFs to better illustrate the data distribution and indicate that the data is sparse at high velocities, and additionally add figure labels to each plot as suggested.

The reviewer is also correct that the models do diverge in some catchments, with the most prominent divergence found in catchment 7 and 8. This divergence suggests the traction relationship could be either rates strengthening or Mohr-Coulomb-like at high velocities. This uncertainty is addressed and acknowledged in section 4.2.1.

**Comment:** Figure 8: Doesn’t the fact that strong and weak beds exist roughly equally in slow and fast flow regions show that bed strength is not related to velocity? If so, then a sliding relation that equates the two falls apart.

**Response:** Since weak and strong beds are defined relative to the ice-sheet wide relationship through the entire velocity range, by this definition, we should expect a similar proportion of weak and strong beds in slow- and fast-moving regions. As such, we agree with the reviewer that it was confusing to put the distribution of weak and strong beds from fast- and slow-moving regions on a prominent spot in the figure. We removed this from Figure 8 and took out the associated text. However, on a physical level, weak-bedded slow-flowing regions can occur in cavitation range of hard-bed sliding (Gagliardini et al., 2007). This is the region of increased curvature before reaching  $CN$  on the black curve of Figure 3. Here, you can have lower traction for a given sliding speed compared to a Weertman relationship while still locally balancing the gravitational stress.

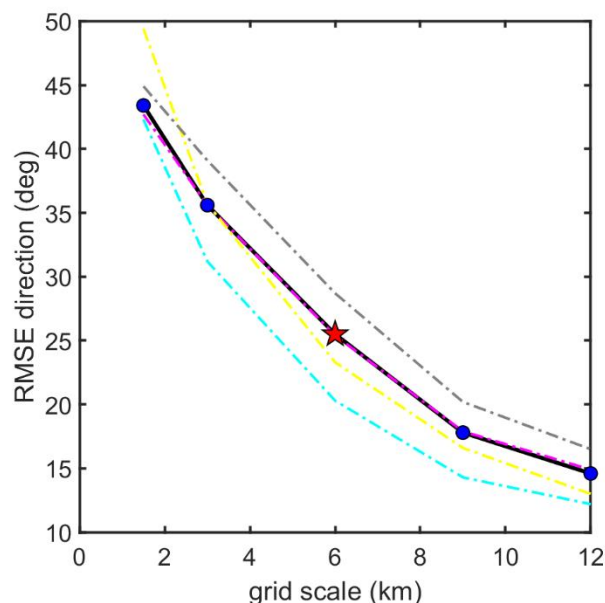
### Additional Comments from the Editor

**Comment:** 1. In regard to filtering driving stress prior to inversion, please consider the recent study of McCormack et al. in Polar Research: <https://polarresearch.net/index.php/polar/article/view/3498>

**Response:** McCormack et al. 2020 presented a method to optimize the driving stress length scale by comparing the direction of the velocity and driving stress vectors. When the direction difference is minimized, it can be assumed that the length scale is sufficient where effect of stress gradients on the flow field are minimized. This is a different, but highly analogous approach to our optimization method which compared the difference SIA and SSA presented in section 2.3. Even though they are similar, our method has a distinct advantage in situations where longitudinal stress gradient coupling dominates the higher-order stresses. Here, the driving stress and flow vectors could still be aligned with significant longitudinal stress gradients, and thus incorrectly suggest the influence of stress gradients is minimized at a given length scale.

Following their study, we also compared the direction of the driving stress vector to the velocity for different filter sizes (Figure R4). We find the RMSE difference in the driving stress and velocity vectors is probably best minimized at 9 km over the entire study area. However, the optimal length scale for our analysis also took into consideration the spatial resolution near the margin and total velocity range over which the velocity and traction could be compared. This is important since many of the defining flow characteristics of the traction laws presented in Figure 3 are expected to occur at high velocities which are found near the margins. Thus, we chose 6 km for analysis, but also included our analysis done with 9 km in the supplemental (Figure S3) which would be interpreted almost identically in terms of predominate bed physics in each catchment.

We note that our surface elevations were smoothed using a Gaussian filter which was found to generally outperform the triangular and bilinear filters tested in McCormack et al. 2020. While we use a spatially



invariant filter in our analysis, McCormack et al 2020, found that beyond  $4H$ , they performed similarly to filters that scaled with ice thickness.

**Figure R4** – Comparison of grid scale to the RMS error of the driving stress vector direction compared to the velocity vector direction. Dashed lines show same analysis for different subsets of the data (margin regions  $< 1200$  m.a.s.l. – yellow line, interior regions  $> 1200$  m.a.s.l. – grey line, thickness  $> 1500$  m – magenta line, thickness  $< 1500$  m – cyan line).

**Comment:** 2. In regard to the \*likely\* basal thermal state, given the rigor with which the authors consider the uncertainties in other elements, I was surprised that the authors did not consider two alternative scenarios: A. The uncertain region is frozen. B. The uncertain region is thawed. Perhaps only the latter scenario is relevant to the methods employed by this study, but as the lead author of the basal thermal state investigation, I caution against prescribing too much confidence in our knowledge of that boundary condition yet.

**Response:** This is a good suggestion and is something we overlooked. We re-ran the analysis to include the uncertain regions of the likely basal thermal state map (Figure R5). By comparing the figure below to Figure 3 in the main text, we can see the uncertain regions are almost universally slow flowing and thus inclusions of the uncertain regions have little impact on our analysis. The exception to this is catchment 3, where the uncertain regions occupy can occupy relatively fast-flowing regions (up to  $\sim 80$  m/a). Here, the uncertain regions have exceptionally high tractions for their velocity. This would be consistent with the uncertain regions being frozen.

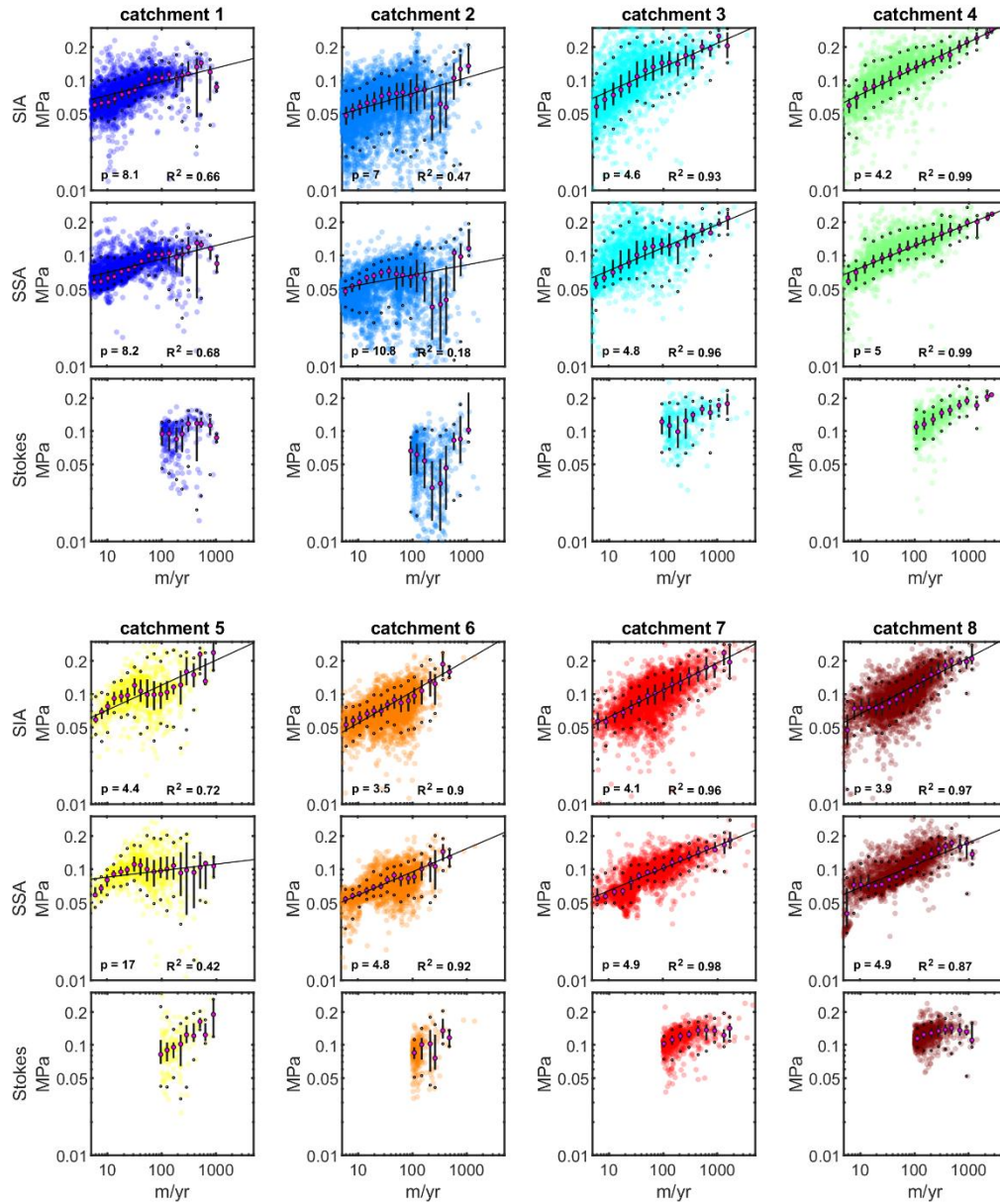


**Figure R5** – The velocity – traction relationship for the SIA , SSA, and Full Stokes inversions (6 km) including the uncertain regions of the basal thermal state mask. Transparency is an indicator of data density, where opaque areas indicate four or more grid cells occupy the same marker area on the plot. Magenta markers show the median traction values for 20 logarithmically spaced velocity bins, the vertical bars show the interquartile range, and the black dots indicate the middle 90 percentile of the data. Black line shows a power law model fit to the binned data. No models were fit to the stokes relationships due to the velocity range (> 100 m/yr) which is limited in our analysis.

**Comment:** 3. Aschwanden et al. (2016) used a bed rheology that depends partly on bed elevation and found that it worked well for their PISM simulations. Please consider the relevance of that study to your

investigation, and perhaps even evaluate even if there is a relation between inferred strong/weak beds and bed elevation.

**Response:** Aschwanden et al. (2016) found using bed elevation as an ad hoc way to tune the sliding relationship helped better capture ice flow and ice speeds within marine-terminating regions of the ice sheet. While not explicitly tied to physics, the justification is that in regions where the bed elevation is below sea-level, sea-level sets the basal pressures and the pressure dependency of the sliding relationship.

The distribution of weak beds and their relationship to hydrology and elevation is examined in detail in a follow up manuscript that is currently submitted (authored by Maier and Gimbert). However, since our relationships are mostly for grounded regions we wouldn't expect a strong dependence on bed elevation on bed strength over much of our study regions given the physical justification for the parameterization. There are some exceptions, the most obvious being the Humboldt and Petermann Glaciers, which have partially floating ice tongues and the Northeast Greenland Ice Stream where the area approximately enveloped by the 200 m/yr contour is below sea level. These regions are classified as weak bedded and would be consistent with the parametrization of hydrology used in the PISM experiment. The same interpretation that inspired the ad-hoc elevational relationship is suggested in our manuscript in lines 409-413:

However, for the low-velocity weak-bedded grid cells, quick comparison to the bed elevation map (Morlighem et al., 2017) indicates they are likely not related to elevation, and instead, seem to be more closely related to the onset of surface melting near the snowline in catchment 6. This is detailed in lines 431 to 438.

## References

- Armstrong, W. H., Anderson, R. S., & Fahnestock, M. A. (2017). Spatial patterns of summer speedup on south central Alaska glaciers. *Geophysical Research Letters*, *44*(18), 9379–9388.
- Aschwanden, A., Fahnestock, M. A., & Truffer, M. (2016). Complex Greenland outlet glacier flow captured. *Nature Communications*, *7*(1), 1–8. <https://doi.org/10.1038/ncomms10524>
- Carr, J. R., Vieli, A., Stokes, C., Jamieson, S., Palmer, S., Christoffersen, P., Dowdeswell, J., Nick, F., Blankenship, D. D., & Young, D. A. (2015). Basal topographic controls on rapid retreat of Humboldt Glacier, northern Greenland. *Journal of Glaciology*, *61*(225), 137–150.
- Dehecq, A., Gourmelen, N., Gardner, A. S., Brun, F., Goldberg, D., Nienow, P. W., Berthier, E., Vincent, C., Wagnon, P., & Trouvé, E. (2019). Twenty-first century glacier slowdown driven by mass loss in High Mountain Asia. *Nature Geoscience*, *12*(1), 22–27.
- Gagliardini, O., Cohen, D., Råback, P., & Zwinger, T. (2007). Finite-element modeling of subglacial cavities and related friction law. *Journal of Geophysical Research: Earth Surface*, *112*(F2). <https://doi.org/10.1029/2006JF000576>
- Habermann, M., Truffer, M., & Maxwell, D. (2013). Changing basal conditions during the speed-up of Jakobshavn Isbræ, Greenland. *Cryosphere*, *7*(6).
- Hogg, A. E., Shepherd, A., Gourmelen, N., & Engdahl, M. (2016). Grounding line migration from 1992 to 2011 on Petermann Glacier, north-west Greenland. *Journal of Glaciology*, *62*(236), 1104–1114.
- Joughin, I., Abdalati, W., & Fahnestock, M. (2004). Large fluctuations in speed on Greenland's Jakobshavn Isbrae glacier. *Nature*, *432*(7017), 608–610.

- McCormack, F. S., Roberts, J. L., Jong, L. M., Young, D. A., & Beem, L. H. (2019). A note on digital elevation model smoothing and driving stresses. *Polar Research*.
- Morlighem, M., Williams, C. N., Rignot, E., An, L., Arndt, J. E., Bamber, J. L., Catania, G., Chauché, N., Dowdeswell, J. A., & Dorschel, B. (2017). BedMachine v3: Complete bed topography and ocean bathymetry mapping of Greenland from multibeam echo sounding combined with mass conservation. *Geophysical Research Letters*, *44*(21), 11–051.
- Stevens, L. A., Hewitt, I. J., Das, S. B., & Behn, M. D. (2018). Relationship between Greenland ice sheet surface speed and modeled effective pressure. *Journal of Geophysical Research: Earth Surface*, *123*(9), 2258–2278.

# Basal traction mainly dictated by hard-bed physics over grounded regions of Greenland

Nathan Maier<sup>1</sup>, Florent Gimbert<sup>1</sup>, Fabien Gillet-Chaulet<sup>1</sup>, and Adrien Gilbert<sup>1</sup>

<sup>1</sup>University of Grenoble Alpes, CNRS, IGE, Grenoble, France

5 *Correspondence to:* Nathan Maier ([ntmaier@gmail.com](mailto:ntmaier@gmail.com))

**Abstract.** On glaciers and ice sheets, identifying the relationship between velocity and traction is critical to constrain the bed physics that control ice flow. Yet in Greenland, these relationships remain unquantified. We determine the spatial relationship between velocity and traction in all eight drainage catchments of Greenland. The basal traction is estimated using three different methods over large grid cells to minimize interpretation biases associated with unconstrained rheologic parameters used in numerical inversions. We find the relationships are consistent with our current understanding of basal physics in each catchment. We identify catchments that predominantly show Mohr-Coulomb-like behavior typical of deforming beds or significant cavitation, as well as catchments that predominantly show rate-strengthening behavior typical of Weertman-type hard-bed physics. Overall, the traction relationships suggest that the flow field and surface geometry over the grounded regions of the Greenland ice sheet is mainly dictated by Weertman-type hard-bed physics. Given the complex basal boundary across Greenland, the relationships are captured reasonably well by simple traction laws over the entire velocity range, including regions with velocities over 1000 m/yr, which provide a parameterization that can be used to model ice dynamics at large scales. The results and analysis serve as a fundamental constraint on the physics of basal motion in Greenland and provide unique insight into future dynamics and vulnerabilities in a warming climate.

## 1 Introduction

For glaciers and ice sheets the relationship between basal motion, basal traction, and the response to external forcing are fundamental to realistic ice flow modeling. The physics that control the interdependencies between these characteristics is dictated by the properties of the bed. For hard beds basal traction is related to the viscous drag generated as ice slides around bed roughness (Weertman, 1964). Meltwater modulates friction and sliding over hard beds by occupying cavities on the lee-side of bedrock bumps (Gagliardini et al., 2007; Lliboutry, 1968; Schoof, 2005), increasing sliding by reducing the apparent roughness of the bedrock. For deformable till beds the traction and occurrence of basal motion primarily depends on the failure strength of the till which acts as a Mohr-Coulomb material (Iverson et al., 1998; Kamb, 1991; Tulaczyk, 1999; Zoet and Iverson, 2020). Meltwater can weaken deformable beds by increasing pore pressures within the till (Iverson et al., 1998, 2003) and induce bed deformation where there was previously none.

Constraining the type of bed is critical to understanding the dynamic response to future forcing given the difference in the physical processes that control ice motion (Bougamont et al., 2014). In Greenland, the composition of the basal substrate is known to vary significantly. There are both hard and till beds (Booth et al., 2012; Cooper et al., 2019; 35 Dow et al., 2013; Doyle et al., 2018; Harper et al., 2017; Kulesa et al., 2017; Lindbäck and Pettersson, 2015; Lüthi et al., 2002). The exact distribution of each is unknown, but direct observations have shown that they coexist at the regional scale (Booth et al., 2012; Dow et al., 2013; Harper et al., 2017). Hydrologic regimes also vary significantly. In low-elevation regions meltwater is delivered to the bed via supraglacial routing of water into moulins (Smith et al., 2015), while at higher elevations water stored in supraglacial lakes can be suddenly injected into the basal interface 40 during catastrophic lake drainages (Das et al., 2008; Stevens et al., 2015). In other regions, basal melting from high geothermal heat fluxes provides an in situ source of basal water independent of surface melt (Fahnestock et al., 2001).

Given complexity of the basal boundary in Greenland, the roles of different physical processes operating at the base in controlling sliding speeds and surface geometry of the ice sheet at large scales have historically been difficult to quantify. Improvements over the last decade in satellite observations of surface velocity and geometry have made it 45 possible to infer bed properties across ice thickness length scales based on ice dynamics (Gillet-Chaulet et al., 2016; Habermann et al., 2013; Minchew et al., 2016). The main approach is to use time variations in the ice flow and surface geometry to constrain characteristic properties of different bed types (Gillet-Chaulet et al., 2016; Habermann et al., 2013). This approach has been used to infer the apparent sliding exponent at Pine Island Glacier and Antarctica (Gillet-Chaulet et al., 2016), and changes in bed strength underneath Jakobshavn (Habermann et al., 2013). However, using 50 time variations to constrain bed properties is limited to regions where large changes in the surface speeds and ice geometry coincide and cannot be applied to much of the ice sheet where dynamic changes are small.

An alternative way to infer bed properties is to use the spatial distribution of velocity and traction to determine the physical relationship between the variables. A study on Hofsjökul, a small isothermal ice cap located in Iceland, used inverted tractions and sliding velocities to show that the relationship between velocity and traction is consistent with 55 deforming bed physics (Minchew et al., 2016). Yet explicit inverting for basal traction using a shallow approximation or full Stokes representation of the momentum balance yields a traction solution that is non-unique and is dependent on the a priori choice of model parameters including both physical parameters related to ice rheology and parameters within regularization schemes necessary to stabilize the numerical solvers and avoid data overfit (Habermann et al., 2013; Shapiro et al., 2016). The influence of the parameters on traction solution are difficult to evaluate, but are 60 expected to be particularly important where rheologic parameters are poorly constrained which can lead to biases in the interpretations of the bed conditions (Habermann et al., 2013; Joughin et al., 2012).

The non-linear ice rheology dictated by “Glen’s Law” is only known to an approximate degree, but is known to have strong dependencies on ice temperature (Cuffey and Paterson, 2010). The Greenland Ice Sheet has a complex polythermal structure especially near the margin where cryohydrologic warming is pervasive (Harrington et al., 2015; 65 Lüthi et al., 2015). Further, in Greenland the uncertainty of the deformation exponent,  $n$ , is large. Direct estimates of  $n$  range considerably from 2.5 to 4.5 (Bons et al., 2018; Dahl-Jensen and Gundestrup, 1987; Gillet-Chaulet et al.,

2011; Lüthi et al., 2002; Ryser et al., 2014). Other aspects of ice flow such as crevasses that are common in regions of concentrated fast flow (Cavanagh et al., 2017; Lampkin et al., 2013) and in extensional regimes (Poinar et al., 2015), are not accounted for in high-order inversions but could significantly impact the relationship between the velocity field and higher-order stresses (stress gradients). Together, these aspects make it difficult to confidently estimate the rheology to invert for tractions across the Greenland Ice Sheet and use the spatial relationship between basal traction and velocity to infer bed properties. **An initial study found no relationship between velocities and tractions for the fast-flowing outlet glaciers located on the periphery of Greenland (Stearns and van der Veen, 2018) a result which is still under debate (Minchew et al., 2019; Stearns and van der Veen, 2019).**

75 In this study, we compare multi-year averaged surface velocities to the basal traction estimated using three different methods **with differing complexity** over large 6 km x 6 km grid cells (*Figure 1*) to determine the form of the velocity – traction relationship within all eight drainage catchments in Greenland (Zwally et al., 2012). **Our hierarchal approach to infer** the basal traction is designed to minimize interpretation bias associated with parameter choice in numerical inversions. Averaging the traction across large length scales diminishes the role of higher-order stresses and thus the need to correctly prescribe the ice rheology to invert for basal traction. Using the three inversions with different complexity (Shallow Ice Approximation, Shallow Stream Approximation, and Full Stokes), we can determine the length scale at which the influence of higher order stresses is minimized. Further, we can separately identify topographic-scale form drag, which arises from ice flowing around large scale topography (Kyrke-Smith et al., 2018), **from skin drag**, which is the component of the basal resistance dictated by bed properties that are of interest for traction laws. Where the three inversions converge, we can confidently infer the form of the velocity and traction relationship, and where they diverge, we can constrain the range of basal physics possible given the different assumptions within each inversion method. We compare the form of the velocity-traction relationships to expectations given different bed physics to interpret the dominant basal processes operating at the catchment scale. Finally, we discuss the implications of the results for current and future ice dynamics in Greenland.

## 90 **2 Methods**

### **2.1 Data**

All three inversions use identical surface elevation, bed elevation, and surface velocity data sets (*Figure 1*). We use the GIMP digital elevation model of the ice sheet surface (30 m resolution) (Howat et al., 2014, 2017) and ice thicknesses and bed topography from BedMachine v3 (150 m resolution) (Morlighem, 2018; Morlighem et al., 2017). We use surface velocities from a multi-year velocity mosaic (250 m resolution) with complete coverage of Greenland (Joughin et al., 2016, 2018) and low absolute errors (generally < 3 m/yr). The velocities represent decadal-scale averages generated from data collected from 1995 – 2015 but are mostly derived from data from 2005 – 2015. The time averaging of velocities incorporates both summer and winter flow, and thus they are not expected to reflect a strong seasonality (Joughin et al., 2018). To ensure high data fidelity we exclude regions where the error and uncertainty in either the velocity or driving stress exceeds 50% of its magnitude (supporting *Figure S7*). We restrict our analysis to thawed regions of each catchment where basal motion is expected to occur. This is delineated using a

map of the basal thermal state (*Figure 1*) (MacGregor et al., 2016, 2017) which delineates thawed, frozen and uncertain regions. We note our results do not significantly change if the uncertain regions are included in the analysis (*supporting Figure S1*).

## 105 2.2 Basal Traction Inversions

### 2.2.1 Shallow Ice Approximation

The Shallow Ice Approximation (SIA) neglects higher-order stresses and thus assumes that the basal traction as equivalent to the gravitational driving stress (Morland and Johnson, 1980). The SIA is valid when the influence of stress-gradient coupling, which arises from spatially complex flow, is negligible, i.e. typically across length scales of roughly 10 ice thicknesses (Cuffey & Paterson, 2010; Kamb & Echelmeyer, 1986), and also where the effects of topographic scale form drag are small, i.e. where the bed is mostly flat. While simple, the SIA does not require the use of unmeasured parameters for either the ice rheology or regularization schemes.

We calculate the driving stress across 6 km length scales where the effect of higher-order stresses is minimized using:

$$\tau_d = \rho_i g H t \alpha = \tau_{b,SIA}, \quad (1)$$

115 where  $\rho_i$  is the density of ice (900 kg/m<sup>3</sup>),  $H$  is the ice thickness,  $g$  is the gravitation constant (9.81 m/s<sup>2</sup>), and  $\alpha$  is the surface slope, which is calculated by taking the gradient of the surface elevations. Prior to the calculation, data sets are filtered with a 6 km x 6 km Gaussian kernel with a sigma optimized to minimize the difference between the SIA and SSA (Shallow Stream Approximation) estimates of traction. The choice of length scale is discussed further in 2.3. We decimate the driving stress and velocity data sets to 6 km grid spacing to generate independent cells. We scale the estimates of driving stress with the surface area of the bed in each grid cell to account for topographic variations which are needed to estimate skin drag (i.e. tangential tractions). This is equivalent to a shape factor commonly used for alpine glaciers (Cuffey and Paterson, 2010).

### 2.2.2 Shallow Stream Approximation

125 The Shallow Stream Approximation (SSA) solves the vertically integrated form of the momentum balance in two dimensions which accounts for higher-order stresses that arise from gradients in the velocity field assuming shearing of the ice column is negligible (MacAyeal, 1989). This approximation is most valid for fast ice flow where shearing is limited or concentrated near the base. The method also implicitly assumes that interactions with the bed besides tangential tractions are negligible and does not explicitly account for topographic-scale form drag. The SSA is therefore most appropriate in regions where the bed topography is relatively flat.

130 The SSA inversion was implemented in Elmer/Ice, a three-dimensional finite-element ice modeling software (Gagliardini et al., 2013; Goelzer et al., 2017). The inversion domain consists of a triangular element mesh with resolution ranging from 500 m to 5 km across the ice sheet domain (*Figure 1*). The model uses an ice rheology with

a vertically averaged viscosity generated from ice temperatures from a paleo-spin-up of the SICOPOLIS model and  $n = 3$  (Goelzer et al., 2017; Seddik et al., 2012). The basal traction was inverted using the control-inverse method with  
135 a linear sliding law to find the “effective” friction coefficient which optimized to minimize the misfit between the observed and modeled velocity (Gagliardini et al., 2013; Morlighem et al., 2010). This friction coefficient includes all the physical dependencies between sliding and tractions. While a linear sliding law is used for the inversion, the traction field is shown to have little sensitivity to the choice of sliding law (Joughin et al., 2004).

### 2.2.3 Full Stokes Inversion

140 The Full Stokes (FS) continuum equations represent the full momentum balance without simplifying assumptions. This means the traction inversions are made in full consideration of vertical shearing of the ice column, higher-order stresses, and topographic form drag as the ice flows around landscape-scale roughness.

The FS inversion is also implemented in Elmer/Ice on a variable-resolution triangular element mesh with fine resolution (~150 m) near the margin and coarse resolution within the interior (~ 60 km) (Gagliardini et al., 2013;  
145 Goelzer et al., 2017). The large grid dimensions in the interior reduce the high computation costs of the FS, which allocates more resources near the margin where ice flow is more complex (*Figure 1*). The ice rheology is calculated using ice temperatures from the SICOPOLIS paleo-spin-up for use in ISMIP6 and  $n = 3$  and the basal traction was inverted using the same methods as the SSA. For consistency with the other inversions, we compare the FS traction field against the surface velocity in our analysis and instead of the inverted sliding velocities. The results are  
150 very similar in both cases and do not change the interpretations presented in the manuscript (see *supporting information*).

### 2.3 Length scale for grid cells

We compare the traction estimates for grid cells with different dimensions to determine at what length scale the effects of higher-order stresses are small, and correspondingly the biases associated with rheology choice in the numeric  
155 inversions are also small. To do so we compare SIA traction computed across grid cells with dimensions of 1.5 – 12 km to the traction from the SSA averaged across the same grid cells (*Figure 2*). We use SSA instead of the FS inversion as it does not explicitly include bed interactions beyond traction, thus differences in the comparison to the SIA traction estimates can be attributed solely to higher-order stresses. We find that averaged over length scales of 6 km, the mean difference between the two traction estimates on average is less than 0.016 MPa (Figure 2) which on average is ~17%  
160 of the traction. The mean difference is similar for marginal (<1200 m.a.s.l.) and interior flow (>1200 m.a.s.l.) and thick (>1500 m) and thin (<1500 m) ice (*Figure 2*) showing the length scale appropriate for a wide range of glaciological settings. This is consistent with previous work which found spatially invariant filters can be used to estimate the driving stress for various ice thicknesses as long as the filter length is sufficiently long (McCormack et al., 2019). Increasing the length scale beyond 6 km does further decrease the difference between the data sets, however,  
165 does not change the data interpretations presented in the manuscript, which we note are also similar if a 3 km length scale is used (*supporting Figure S2, S3*). We choose to use 6 km grid cells in the analysis in order to maximize the

170 resolution near the margins, lengthen the span of velocity and traction range used to determine the relationship between the variables, and provide more interpretable relationships in catchments 3 and 5 which have fewer grid cells. Like the SSA, the FS tractions are averaged across the 6 km grid cells for this analysis. Due to the coarse nature of the interior grid cells for the FS simulation, we only use grid cells where velocities are greater than 100 m/yr which conservatively delineates where the mesh resolution is less than the 6 km limit (*Figure 1*).

## 2.4 Interpreting the Velocity-Traction Relationships

### 2.4.1 Physical Traction Relationships

175 The theoretical relationship between velocity and traction for idealized beds have characteristic features that can be used to distinguish between different types of basal physics. Below we outline three types of beds and the diagnostic features that we will use to aid our characterization of the basal physics in each catchment.

*Hard bed (Weertman 1964)*: Weertman sliding describes the velocity-traction relationship for ice sliding around bed roughness without cavitation:

$$\tau_b = \left( \frac{u_b}{A_s} \right)^{1/m}, \quad (2)$$

180 where  $A_s$  is a friction factor that incorporates the basal roughness characteristics as well as the near basal ice rheology,  $u_b$  is the sliding velocity, and  $m$  is the sliding exponent. This is a rate-strengthening relationship where increasing sliding result in increasing stress (*Figure 3*).

*Hard bed with cavitation (Gagliardini 2007)*: A hard bed relationship that includes cavitation combines aspects of both rate-strengthening and Mohr-Coulomb-like behavior given by:

$$185 \quad \tau_b = CN \left( \frac{X}{1+\alpha X^q} \right)^{1/n}, \quad (3)$$

where  $\alpha$  is a function of  $q$  and  $X = \frac{u_b}{C^n N^n A_s}$ . Here  $q$  is a bed shape parameter,  $C$  a parameter related to the steepness of the bed roughness,  $N$  is the effective pressure at the bed,  $A_s$  is friction factor comparable to that in the Weertman relation, and  $u_b$  is the sliding velocity. Here, rate strengthening occurs at high effective pressures producing a relationship identical to Weertman sliding (*Eq. 2, Figure 3*). When  $CN$  is approached the curvature of the relationship begins to increase, deviating from Weertman behavior. This continues until  $CN$  is reached which is commonly known as Iken's bound (Iken, 1981). Further increases beyond Iken's bound would cause the basal drag to decrease (rate-weakening) causing the ice flow to unstable in the absence of higher-order stresses. However, outside of rare instances leading to glacier collapse (Kääb et al., 2018), glaciers remain stable because sliding and traction in this range is controlled non-locally by higher-order stresses.

195 *Deformable Bed (Zoet 2020)*: Traction for deformable beds combines rate strengthening and Mohr-Coulomb behavior. Below the strength of the till basal motion occurs as over a hard bed (same as described in *Eq. 2*), occurring at the interface between the ice and the till as the ice deforms around bed roughness. Once the basal traction reaches the yield stress ( $\tau_*$ ) till deformation begins. Further increases in stress are limited and the velocity becomes independent of the stress, which like with cavitation, is dictated non-locally by higher-order stresses. This produces a characteristic sharp kink in the velocity traction relationship at the yield stress of the till (*Figure 3*). Over the large grid cells used in this analysis the gravitational stress is mainly balanced by the basal traction. For grid cells with mostly deforming beds this means higher-order stresses will only play a minor role in the stress equilibrium but ice flow in the surrounding regions will still control the velocity field. This same logic applies for the rate-weakening range for hard beds with significant cavitation.

## 205 **2.4.2 Deformation Motion**

The surface velocity reflects the combined motion due to basal motion and internal ice deformation and thus interpretation of the derived relationships requires consideration of both components of motion. In Greenland, the rheologic uncertainty and complex thermal structure make it difficult to infer a location specific rheology to confidently calculate deformation across the ice sheet (Maier et al., 2019). However, direct measurements of basal motion collectively show the prevalence of high fractions of basal motion [0.44 – 0.96] across a wide range of glaciological environments in Greenland (Doyle et al., 2018; Lüthi et al., 2002; MacGregor et al., 2016; Maier et al., 2019; Ryser et al., 2014).

Nevertheless, we demonstrate the relationship between surface velocity and traction remains interpretable in terms of bed properties even if deformation motion contributes significantly to the surface velocity and/or the parameters that controls the rate of deformation change significantly towards the margin. In *Figure 3* we add deformation motion to the traction relationships presented in 2.4.1 for a temperate ice column with a thickness of 2500 m using:

$$u_d = \frac{2A(T)}{n+1} \tau_b^n H, \quad (4)$$

where  $A(T)$  is a temperature dependent rate factor (calculated following Cuffey and Paterson 2010),  $n$  is the flow law exponent equal to 3, and  $\tau_b$  is the basal traction as dictated by the relationships in *Figure 3*. This corresponds to a deformation fraction of 0.33 for the rate-strengthening range of the traction relationships, which is similar to that measured along the margins (Doyle et al., 2018; Lüthi et al., 2002; MacGregor et al., 2016; Maier et al., 2019; Ryser et al., 2014), and would approximate deformation where changes in flowline ice thickness are small, i.e. some trough-bound outlet glaciers. We show the characteristic features of the relationship are identical as to the theoretical relationships which relate basal motion to traction. We then test how systematic changes in deformation motion due to marginal thinning or ice warming, which is documented as ice moves from the interior to the margin (Harrington et al., 2015; Lüthi et al., 2015), could influence the traction relationship. We find that even with large marginal ice thickness (3000 – 200 m) and ice temperature changes ( $-25^\circ - 0^\circ$ ) occurring through the velocity range, the

characteristic features of the traction relationships remain unchanged. The persistence of the traction relationships with added deformation motion arises from the strong and non-linear dependence of deformation motion on the basal traction which is controlled by the properties of the bed. Thus, we can interpret the characteristic features that define each type of bed-physics using surface velocities which remain clearly distinguishable even with deformation motion.

### 2.4.3 Power-law model fitting

We fit a general flow approximation to the observed surface velocity ( $u_s$ ) and traction range in each catchment using:

$$\tau_b = C_p u_s^{\frac{1}{p}}, \quad (5)$$

where  $C_p$  is a rate parameter and  $p$  is an apparent flow exponent. Since the surface velocity reflects the combined motion due to internal ice deformation and basal motion this equation approximates the combined physics and nonlinearities of each flow mechanism. However, as shown in *Figure 3* the main features of the traction relationships, and therefore the model fit, will be dictated by the basal physics.

We use the magnitude of  $p$  as an additional indicator of basal physics and hydrologic influence to interpret catchment dynamics (Joughin et al., 2019). Frozen beds are expected to have  $p$  approximately equal to the deformation exponent  $n$ . The regelation and creep processes (Cuffey and Paterson, 2010; Weertman, 1964) that dictate hard bed sliding suggest  $m \approx 2.5 - 3$  for  $n = 3$ , which is similar to that expected over frozen beds. However, when cavities form on the lee side of bedrock bumps as in *Eq. 3*, the apparent sliding exponent  $m$  and thus  $p$  have the potential to increase beyond this range due to decreased ice-bed contact area (Gagliardini et al., 2007; Joughin et al., 2019), which increases curvature in the velocity-traction relationship (Gagliardini et al., 2007; Joughin et al., 2019). For deforming beds  $p$  is expected to be large to approximate Mohr-Coulomb behavior (Iverson et al., 1998; Kamb, 1991; Tulaczyk et al., 2001). This is supported by in-situ field (Gillet-Chaulet et al., 2016) and laboratory (Kamb, 1991) experiments which show  $m \geq 20$  over deforming beds.

We fit the model to the binned velocity – traction relationship in the thawed and frozen regions of each catchment (number of bins = 20, logarithmically spaced) using a nonlinear least-squares regression in *MATLAB*. Fitting the binned data gives equal weights to fast flowing and slow-flowing regions of each catchment regardless of the amount of grid cells of each. We do not fit models to the FS tractions which we limit to velocities above 100 m/yr and do not reflect the full velocity range. We note that velocity and traction magnitudes are dampened due grid cell averaging, thus the binned-relationships and model fits will reflect this range rather than the full range possible in each catchment.

## 3. Results

### 3.1 Relationship between velocity and basal traction

The velocity versus traction relationships have a large degree of scatter but show increasing velocities result in increasing traction (*Figure 4, supporting Figure S4 – linear scale*). The relationship between the binned variables (magenta dots) is visually well defined in all catchments and for each estimate of traction. In general, there is good agreement with the binned data and model fit at both high and low velocities. The  $R^2$  is high in catchments 3, 4, and 6 through 8 [0.88 – 0.99] indicating that the power-law model generally describes most of the variability of the binned relationships (*Figure 4, supporting Table S1*) for the SIA and SSA tractions. In the remaining catchments (1, 2, and 5) the  $R^2$  is lower [0.22 – 0.69], which results from the increasing curvature in the binned data at higher velocities which is not captured with the power law. With the exception of catchment 2, 3 and 5, the interquartile range (IQR) for each bin occupies a small region of the total data spread indicating the binned relationships represents a large fraction of the data in each catchment.

The relationships for SIA, SSA, and FS inversions show varying degrees of consistency in each catchment (*Figure 5*). In general, the different inversion methods show the same traction variations through the velocity range but show some offset in the basal traction. Bins with offset between the SIA and SSA suggest higher-order stresses may influence tractions, while bins with offset between the SSA and FS suggest topographic scale roughness may support some of gravitation stress through form drag. All catchments show offset between the SIA and SSA at some bins, however, the offset is small (generally < 0.02 MPa). Similarly, catchments show some differences between SSA and FS. In catchments 6 through 8, we find the relationships increasingly diverge as velocities increase, where peak separation between the SIA, SSA, and FS coincides with the highest velocities.

The binned velocity-traction relationships (*Figure 5*) all have one or more of the characteristic features found in the theoretical traction relationships presented in *Figure 3*. In catchment 1 and 2 there is rate-strengthening until a visible kink in the traction relationships at ~0.1 MPa and ~0.08 MPa respectively where tractions level off. In catchment 2 this is followed by a large dip in the traction relationship where tractions decrease to a local minimum at ~230 m/yr. In both Catchment 1 and 2, the highest velocities again correspond with high tractions which fall on a similar trend as the binned relationship before the kink. Catchments 3 and 4 show rate-strengthening through the entire velocity range. Catchment 5 shows rate-strengthening until ~ 40 m/yr where tractions abruptly dip until ~60 m/yr. The SIA and FS then begin to increase again at a similar rate as before the dip but offset towards higher velocities, while the tractions for the SSA level off at ~ 0.095 MPa. Catchment 6 predominantly shows rate strengthening, with a small kink at ~50 m/yr which corresponds with an increase in data scatter and IQR span. Catchment 7 also predominantly shows rate strengthening but at high velocities (440 m/yr) the relationships for the different inversions diverge: the SIA continues rate strengthening, the SSA has a kink where tractions level off, and the FS tractions decrease. Catchment 8 is almost identical to 7 which shows rate-strengthening until ~480 m/yr where after the traction estimates diverge. However, Catchment 8 also has a small kink that occurs at ~20 m/yr.

### 3.2 $p$ magnitude

The averaged flow exponent (calculated using the combined mean of SIA and SSA) within the likely frozen regions is 2.9 [2.4 – 4.1] which is expected to approximate  $n$  (*Figure 6, supporting Figure S5*). In all catchments  $p$  of the

thawed regions exceeds the approximate  $n$  to varying degrees [4.0 – 10.6] suggesting the influence of processes that increase the nonlinearity of ice flow at the catchment scale. The highest  $p$  [ $> 8.1$ ] are recorded in the two northernmost and the southernmost catchment driven by a strong increase in curvature and abrupt dips in traction as velocities increase (Figure 5). However, for catchment 5 high  $p$  and increased curvature only occur for the SSA traction estimates.  $p$  of this magnitude cannot be explained through systematic variations in  $n$  (supporting information), and thus is consistent with the influence of basal processes (i.e. deforming till, cavitation, roughness) on catchment-scale dynamics (Gagliardini et al., 2007; Kamb, 1991). The binned traction relationships and associated  $p$  in the remaining catchments (3, 4, 6 – 8) are similar.  $p$  is approximately 4.4 [4.0 – 4.9] indicating a modest increase in nonlinearity compared to the frozen regions. The changes in the deformation fraction as ice warms or thins towards the margin shown on Figure 3 are unlikely to produce a greater than  $\sim 0.15$  change in  $p$  from  $n$ , and thus even though small, the increase in  $p$  is unlikely to be due to systematic deformation variations. This suggests a modest influence of basal processes or rheologic variations that would increase  $p$  from  $n$  (supporting information).

### 3.3 Spatial distribution of strong and weak beds

We map the distribution of weak and strong beds across the GrIS using the residual distribution from the ice sheet-averaged flow relationship derived from the mean of the three traction estimates (Figure 7, 8). We classify strong and weak beds as data that comprise respectively the top and bottom 15% of the distribution respectively, while the middle 70% of the data is classified as having normal strength (Figure 7). In other words, strong beds have a higher than normal traction for a given velocity, while weak beds have lower than normal traction for a given velocity, and thus the classification is independent of substrate type. By using the mean traction, information from all three traction methods is incorporated and thus weak and strong beds will occur most frequently where the traction estimates agree on the bed strength. We note that the variability used for this designation is far greater than that expected from data error and uncertainty (supporting information, supporting Figure S6) and thus represents real spatial variations in basal characteristics. We compare the spatial variability in bed strength to the distribution of fast and slow-moving ice defined as those moving greater and less than 200 m/yr respectively, as well as the decadal-averaged snowline which serves as a time-integrated proxy for the equilibrium-line altitude (Vandecrux et al., 2019).

The ice-sheet wide distributions of strong and weak regions show the majority of the ice sheet domain is of average strength with aggregated regions of strong and weak beds distributed in select locations (Figure 8). This general description applies for both the slow and the fast-moving regions of the ice sheet, including the three largest glaciers in Greenland: Jakobshavn Isbræ, Kangerlussuaq glacier, and Helheim glacier (Shapiro et al., 2016). There are only a few visually aggregated weak-bed regions across the GrIS. The largest region occurs in catchment 2 within the bounds of the Northeast Greenland Ice Stream (NEGIS). Aggregated weak beds also occur in catchment 6 directly downgradient from the snowline suggesting meltwater forcing is likely important to their occurrence. Aggregated strong beds occur in catchment 4 and catchment 8. In catchment 4 these primarily occur along the thawed-region boundary and could be due to the basal thermal state being misclassified or locally elevated stress coupling that arises near the transition to sliding. The strong bed regions in catchment 8 occur below the snowline near and are therefore

less likely to be misclassified or strongly coupled to frozen regions. We suggest they could instead be related to rougher topography (*Figure S8*) or possibly subglacial drainage conditions near the margins.

330 Catchments 3, 4, and 8 have the highest proportion of strong beds, while catchments 2 and 6 have the highest fraction of weak beds and are the only catchments with a higher proportion of weak beds than strong beds (*Figure 8*). We find an equal percentage of weak bed and strong bed (21%) grid cells in fast – flowing regions and in the slow-moving regions the proportions are roughly equal (14 – 13%) as well. **This is expected since our designation of weak and strong beds occurs through entire velocity range.**

## 4. Discussion

### 335 4.1 Physically based traction relationships

We show that physically based velocity – traction relationships can be retrieved from the ice dynamics of Greenland. This should give confidence that our current descriptions of basal physics, where stresses are related to velocity, are appropriate to model ice motion across much of the ice sheet. We find that in most catchments the binned velocity and traction has characteristics that are expected given our understanding of basal physics and moreover, can be well  
340 represented with a generic power-law traction relationship with varying exponents at high and low velocities. This provides a simple, catchment-specific parameterization that can be used to model the flow field and tractions at large scales **which could be directly prescribed for SIA and SSA simulations (discussed in more detail in 4.4, model parameters provided in supporting Table 1).**

Our finding of gravity-driven flow is the opposite result of an analysis by Stearns and van der Veen 2018 which found  
345 no relationship between traction and velocities for tidewater outlet glaciers on the periphery of Greenland. The two analyses are fundamentally different both in terms of methodology and scope making a straightforward comparison difficult. The coarse grid spacing needed to infer the basal traction and the catchment-scale approach presently used mean our data-derived relationships dominantly reflect the grounded regions of the ice sheet. However, the large, partially floating ice tongues of the Humboldt (Carr et al., 2015) and Petermann (Hogg et al., 2016) glaciers in  
350 catchment 1 are resolved by our method and are found to be underlain by anomalously weak beds (*Figure 8*). This suggests tidewater regions might have mostly Mohr-Coulomb-like behavior and therefore our observations do not directly contradict the previous findings (Stearns and van der Veen, 2018). Nevertheless, most of high-velocity **regions inland from** the calving face of Jakobshavn Isbræ, Kangerlussuaq glacier, and the Helheim glacier do show reasonable adherence to the derived flow relationships, which was not previously found (Stearns and van der Veen, 2018).

### 355 4.2 Interpretation of catchment-scale dynamics

**Each catchment covers a large area where varying bed properties are likely. We use the characteristics of the binned relationships,  $p$ -values, scatter, and the distribution of weak- and strong-bed grid cells to interpret and discuss the dominant basal physics that would result in the catchment-scale dynamics observed.** We note that tractions for hard-bed sliding with cavitation and deforming beds have very similar characteristic features (i.e. strong increase curvature

360 vs. kink). Here we characterize these features as Mohr-Coulomb-like behavior which could reasonably occur over both bed types and only interpret further where additional information permits. We note that our interpretations assume that the binned relationships (and thus model fits) reflect the main characteristics of the traction laws outlined in 2.4.1 as opposed to systematic variations in bed parameters (i.e. roughness characteristics).

#### 4.2.1 Predominantly rate strengthening

365 The binned-velocity traction relationships in Catchments 3 and 4 have all the characteristics of Weertman-type traction laws. There is rate strengthening through the entire velocity range with no large kinks or curvature changes that would indicate Mohr-Coulomb-like behavior is induced either via cavitation or deforming till (*Figure 5*). Correspondingly,  $p$  is the closest to  $n$  for these catchments, indicating only a limited occurrence of higher non-linearity processes operating at the basal interface (*Figure 6*). There are relatively few high velocity low traction grid cells outside the  
370 middle 90<sup>th</sup> percent of the data suggesting that weak beds in these regions are not common (*Figure 4*) and those that do mostly occur within the slower moving regions inland from the margin, with the exception being the very terminus of the Helheim Glacier (*Figure 8*). Given the adherence to rate strengthening in these catchments we can constrain  $CN$  which sets Iken's bound (defined in *Eq. 3*) to be greater than or equal to 2.1 and 2.3 MPa for the SSA and SIA respectively (*Figure 4*). However, other hard-bed parameters cannot not be confidently defined since our binned  
375 relationships are derived from surface velocities which include deformation motion.

To a large degree the relationships in catchments 7 and 8 also adhere to Weertman-type hard bed physics behavior for all three traction estimates below velocities of  $\sim 450$  m/yr, which accounts for greater than 95% percent of the data within each catchment (*Figure 5*). At higher velocities the traction estimates diverge and the interpretation becomes more ambiguous. The SIA continues to show rate-strengthening while the curvature of SSA and FS increase and the  
380 tractions level off. The difference between the relationships indicates that higher-order stresses and/or topographic form drag could influence the defining characteristics of the traction relationship at high velocities which is consistent with the spatially complex flow and bed topography found near the margins (Joughin et al., 2018; Morlighem et al., 2017). The magnitude of these effects is again determined by rheology, and thus the true traction field remains uncertain but could reasonably reflect either rate-strengthening or Mohr-Coulomb-like behavior given the spread in  
385 the relationships at high-velocities.

An increase in Mohr-Coulomb-like behavior at high velocities near the marine-terminating outlets would be consistent with prior traction inversions of the fastest-flowing outlet glaciers in Greenland (Jakobshavn Isbræ, Helheim, Kangerlussuaq) (Habermann et al., 2013; Joughin et al., 2012; Shapero et al., 2016). In general, these inversions have found uniformly weak beds underneath the concentrated regions of fast flow that occur within the deep bed troughs.  
390 Interestingly, these outlet glaciers also correspond to high driving stress which cannot be supported by the inferred weak beds, and thus stress is balanced by  $> 0.5$  MPa traction bands along the margins of the bed troughs which control the flow speeds (Habermann et al., 2013; Joughin et al., 2012; Shapero et al., 2016).

While our analysis by design cannot capture the complex traction field of individual outlet glaciers, we can use our flow relationships to estimate flow speeds expected at tractions of 0.5 MPa and provide a test of the weak-bed hypothesis in these regions using our data-constrained flow relationships. We find that flow speeds at 0.5 MPa would range from ~ 20 km/yr to 100 km/yr (spread from the rate-strengthening catchments). This exceeds the ~ 5 - 10 km/yr velocities that are observed in these regions which would better correspond with tractions ranging from ~0.275 - 0.4 MPa. This suggests short-length scale bed roughness where the high stresses occur may be exceptionally rough and support higher stresses than expected for the given flow speeds, or alternatively the ice in the shear margins is weaker and produce less resistance than expected, and thus beds within the trough may still be weak, but not as weak, or as uniformly weak as previously inferred.

#### 4.2.2 Predominantly Mohr-Coulomb-like

Catchment 1 and 2 both show strong evidence of Mohr-Coulomb-like behavior. In both catchments the average  $p$  is greater than  $> 8.1$  (*Figure 6*), driven by abrupt increases in curvature in the binned velocity - traction relationship which is characteristic of Mohr-Coulomb beds (*Figure 4, 5*). Further, the dip in the binned relationship in Catchment 2 indicates that weak beds make up a substantial fraction of grid cells at high velocities. The abrupt curvature changes occur 0.07 MPa and 0.1 MPA for catchment 1 and 2, respectively, and would correspond to a catchment-mean  $CN$  or  $\tau_*$  depending on whether the bed is hard or deforming (discussed more below).

The distribution of grid cells indicates the beds in each catchment have different characteristics even though they both display Mohr-Coulomb-like traction relationships. In catchment 1, the change in curvature coincides with an increase of high velocity – low traction grid cells (*Figure 4*) which occur within the partially floating ice tongues of the Humboldt and Petermann glaciers (*Figure 8*), indicating that weak beds mainly coincide with areas where the influence of sea-level on basal water pressures can occur (Carr et al., 2015; Hogg et al., 2016). In catchment 2 low traction grid cells occur throughout the entire velocity range and become more dominant at higher velocities (*Figure 4*). Unsurprisingly, they closely coincide with the NEGIS (*Figure 8*) which is known to be underlain by mechanically weak till (Christianson et al., 2014) and has high rates of basal melting from an anomalous geothermal heat flux (Fahnestock et al., 2001), factors which are considered critical to its occurrence (Christianson et al., 2014; Fahnestock et al., 2001; Rogozhina et al., 2016).

#### 4.2.3 Mixed behavior

The binned relationship for catchment 6 is predominantly rate strengthening and has a good fit to the power law models which only show a small increase in  $p$  over  $n$  (*Figure 4 – 6*). Yet the catchment also has the second highest percentage of weak-bed grid cells (*Figure 8*) that sharply increase in occurrence at 60% through the velocity range which coincides with a small kink in the traction relationship (*Figure 4, 5*). Correspondingly, the delineation of the bottom 5% of the data (black markers, *Figure 4*) in each bin also shows a sharp Mohr-Coulomb-like kink. Thus, while there are not enough weak-bed grid cells to significantly impact the median of the binned relationships, weak beds consistent with Mohr-Coulomb-like behavior are clearly present and important to the ice dynamics in this catchment.

Since the relationship has clear attributes of both rate strengthening and Mohr-Coulomb-like behavior through the velocity range we classify this catchment as mixed. This characterization is consistent with direct measurements of basal conditions that have identified both hard and till beds (Booth et al., 2012; Dow et al., 2013; Harper et al., 2017; Kulesa et al., 2017) and persistently low effective pressures that are almost always less than 20% of overburden (Wright et al., 2016).

The weak-bed grid cells mostly occur directly downgradient from the snowline and presumably are linked to the occurrence of hydrologic forcing (Figure 8) which matches previous conclusions of a previous study which identified the weak bed regions as occurring due to the onset of hydrologic forcing (Meierbachtol et al., 2016). In these higher elevation zones, moulins are sparsely spaced (Smith et al., 2015), but large, stochastic, injections of water to the base from supraglacial lake drainages are thought to weaken the bed during the melt season (Das et al., 2008; Kulesa et al., 2017; Stevens et al., 2015). Interestingly, this region is the only region to show a transition to weak beds below the snowline even though supraglacial lakes and meltwater forcing are ubiquitous along the margins of the ice sheet (Leeson et al., 2015).

#### 4.2.4 Unclassified

There is no clear interpretation for the relationship in the catchment 5 which has the fewest grid cells (Figure 1) and the highest ice thickness and velocity errors that are often near 50% magnitude (supporting Figure S7). Unlike the other catchments,  $p$  values for the southernmost catchment are notably different for the SIA ( $p = 4.4$ ) and SSA ( $p = 16.9$ ) (Figure 4). While there is a well-defined kink in the flow relationship, after the kink the SIA and FS again show rate strengthening while the SSA shows Mohr-Coulomb-like behavior (Figure 5). It is generally unclear why the FS has higher tractions, which due to the inclusion of topographic form drag should have lower tractions than the SSA. The kink occurs at low velocity and high stress inland from the ELA (Figure 8), which could reasonably be a result of misclassification of basal thermal state as thawed or a transition to a Mohr-Coulomb-like bed. Given these uncertainties, we refrain from characterizing the catchment in further detail.

#### 4.3 Grounded regions of the ice sheet mainly set by hard-bed physics

The ice-sheet wide velocity-traction relationship exhibits rate-strengthening which is typical of hard-bed physics (Figure 7). This is consistent with the catchment scale results where most of the ice sheet outside of catchment 1 and 2 are generally consistent with a Weertman-type traction law, even regions with ice speeds approaching 1000 m/yr. Our results dominantly reflect grounded regions of the ice sheet where sea-level does not set the reference pressure, yet even so, our results suggest that even near terminus of some of the largest marine-terminating outlets glaciers, hard-bed physics primarily dictates the traction field. The  $p$ -values in the rate-strengthening catchments are greater than expected due to regelation alone ( $p \approx \frac{n+2}{1}$ ) (Weertman, 1964), which indicates the main rate-strengthening process is likely form drag around small-scale bed roughness.

460 We cannot explicitly discriminate between bedrock beds and non-deforming till beds which are expected to have  
identical sliding physics in the rate-strengthening range (Gagliardini et al., 2007; Weertman, 1964; Zoet and Iverson,  
2020). However, comparison to direct observations made via seismic and borehole survey indicate till beds are  
relatively common across the western half of Greenland in regions where we identify the bed to predominantly reflect  
Weertman-type sliding (Booth et al., 2012; Dow et al., 2013; Doyle et al., 2018; Kulesa et al., 2017; Walter et al.,  
2014). Interestingly, these observations contradict radar-derived roughness proxies at the ice-sheet scale that find  
465 significant bed roughness at the  $< 100$  m (Cooper et al., 2019) and km length scale (Lindbäck and Pettersson, 2015;  
Rippin, 2013) which is inconsistent with flat beds typically associated with sediment plains. Thus, there is a  
discrepancy between the local and ice-sheet wide indicators of substrate and our observations of rate strengthening.

To reconcile the observations and the results of our study, we posit that even though till beds appear to be relatively  
common across the grounded regions of the ice sheet, they are either weak and predominantly occur in small patches,  
470 more widespread but mechanically strong, or not always deforming in time. As a result, even across mixed-substrate  
domains, hard-bed physics is **predominantly** manifested in the ice flow field and surface geometry at large scales in  
Greenland. Our assertion of either dispersed and patchy or mechanically strong till beds is supported by the stress  
regimes coinciding with the direct till observations made on the western margin of Greenland. The five field sites  
where till was directly identified indicate overall high bed strength with driving stresses between 0.08 and 0.21 MPa  
475 (Booth et al., 2012; Doyle et al., 2018; Kulesa et al., 2017; Ryser et al., 2014; Walter et al., 2014) (*supporting Table*  
*S2*). Further, the occurrence of multiple observations of hard-bed conditions (Harper et al., 2017) in the same region  
as many of the till observations (Booth et al., 2012; Dow et al., 2013; Kulesa et al., 2017) suggest that till naturally  
occurs in discontinuous patches along the bed which is consistent with our interpretation.

#### 4.4 Implications for Greenland ice flow

480 Our comparison of multi-year velocities and tractions shows the adherence to rate strengthening averaged across  
summer and winter flow which suggests over longer timescales the dynamics at the ice-sheet scale are largely  
determined by the stress at the bed **in most catchments**. Future changes in ice speeds will be dictated by marginal  
thinning, changes at marine-terminating outlets, or changes in the basal hydrology (Alley and Joughin, 2012). Our  
flow relationships are not prognostic at the seasonal to annual time scales where changes in the gravitational stresses  
485 are small and flow variations predominantly reflect changes in the subglacial drainage system or changes at marine  
terminating outlets. Yet, where there are large changes in the traction due to thinning, our flow relationships can  
estimate the corresponding change in dynamics. Using our model parameters from the rate-strengthening catchments  
we estimate the rate at which velocities will change in response to traction perturbations. In fast-flowing regions  
( $\sim 1000$  m/yr) the rate of velocity change is estimated between 15 and 35 m/yr per kPa and in slow regions ( $\sim 200$   
490 m/yr) between 4 and 10 m/yr per kPa (*supporting Figure S9, Table S1*). This serves as an important constraint in  
Greenland where much of the marginal zones are observed to be thinning (Csatho et al., 2014; Mouginot et al., 2019).

Across timescales and in regions where meltwater forcing drives flow variations, one of the most critical  
characteristics that determines how ice flow will respond is whether the bed is hard bedrock or deformable sediment.

495 This property not only sets the type of physics at the bed, but also sets the morphology of the basal drainage system,  
where water either flows at the basal interface through networks of cavities and channels or conversely through the  
pore space of the till (Cuffey and Paterson, 2010). While our analysis cannot explicitly distinguish Mohr-Coulomb-  
like behavior induced by till deformation versus extensive cavitation, we posit that the weak-bed grid cells are  
reasonable candidates for where there could be consistently deforming till beds. Modeling has suggested deforming  
500 till beds are much more likely to experience continued acceleration with increasing melt (Bougamont et al., 2014),  
and correspondingly, these regions could be more vulnerable to increased meltwater forcing in a warming climate.  
Interestingly, there are very few weak-bed grid cells found below the snowline where active meltwater forcing occurs  
except in catchment 6. This is stark contrast with catchments 7 and 8, where bed strength below the snowline is mainly  
normal or strong. This may indicate hydrology has a limited effect on multi-year averaged ice flow outside of select  
regions, but importantly, also reinforces the idea that till beds in other regions outside of catchment 1 and 2 are either  
505 mechanically strong or only sporadically undergo periods of deformation likely during periods of active melt forcing.

## 5. Conclusions

We use multi-year averaged velocities and basal traction estimates to determine the spatial relationship between  
velocity-traction relationship for all eight drainage catchments in Greenland. We show the derived traction  
relationships are consistent with our current understanding of hard and deforming bed physics and that we can clearly  
510 distinguish between predominantly rate-weakening and predominantly Mohr-Coulomb-like behavior in different  
catchments. Overall, we find the flow field and ice geometry of Greenland mostly reflect Weertman-type sliding  
physics across the grounded regions of the ice sheet, with the exception being the NEGIS and partially floating regions  
of the ice sheet which obey expectations given Mohr-Coulomb-like behavior. We use the ice-sheet wide flow  
relationship to identify the location of weak beds which constrains the regions that may have deforming beds that  
515 could be more vulnerable to increased melt in a warming climate. Our work indicates that current and future dynamics  
over grounded regions of Greenland will in a large part depend on Weertman-type hard-bed sliding physics. This  
provides an important constraint for ice sheet modelers and serves as a starting point for future investigations that  
examine location specific bed properties and traction relationships at finer scales.

520

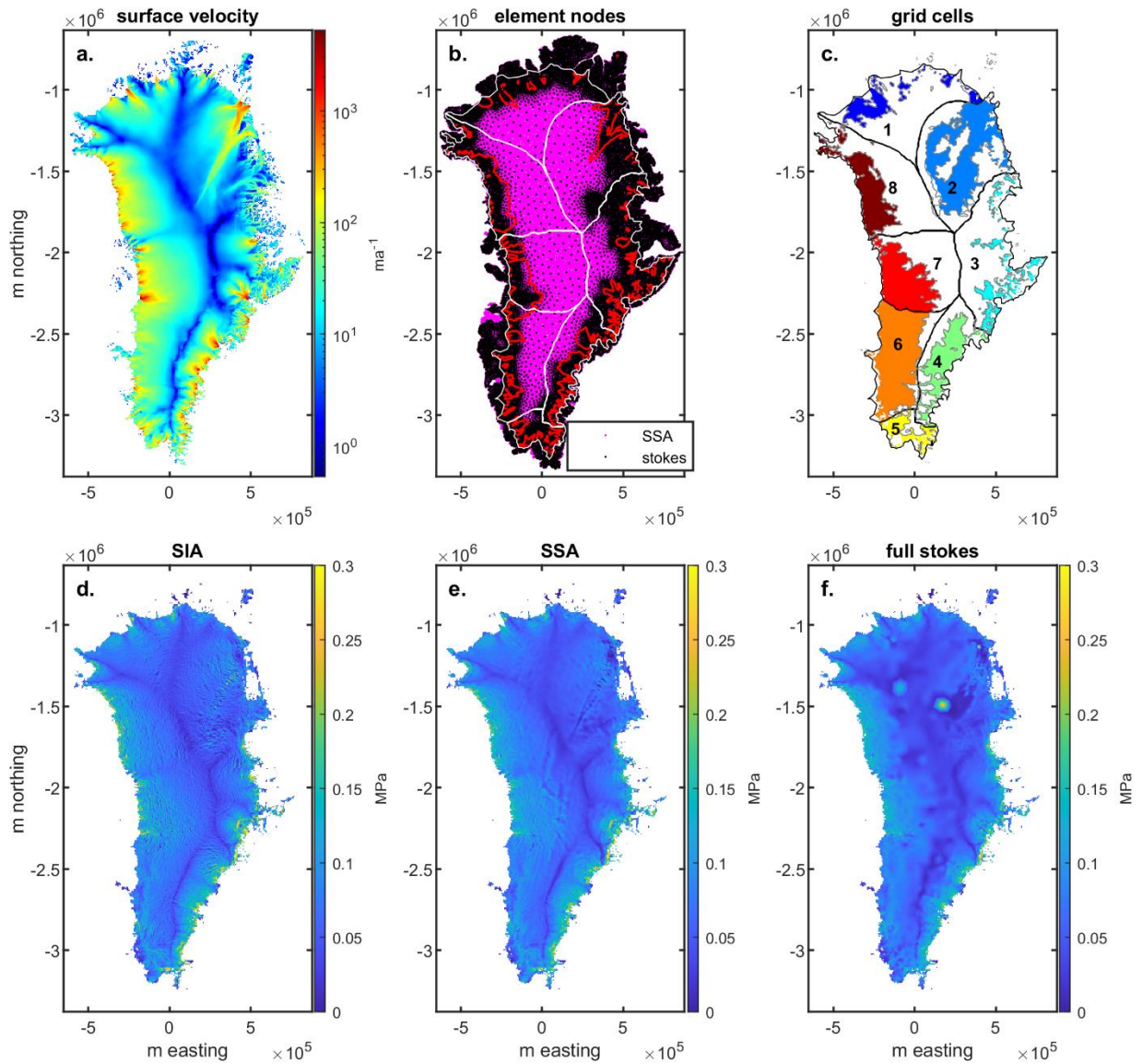
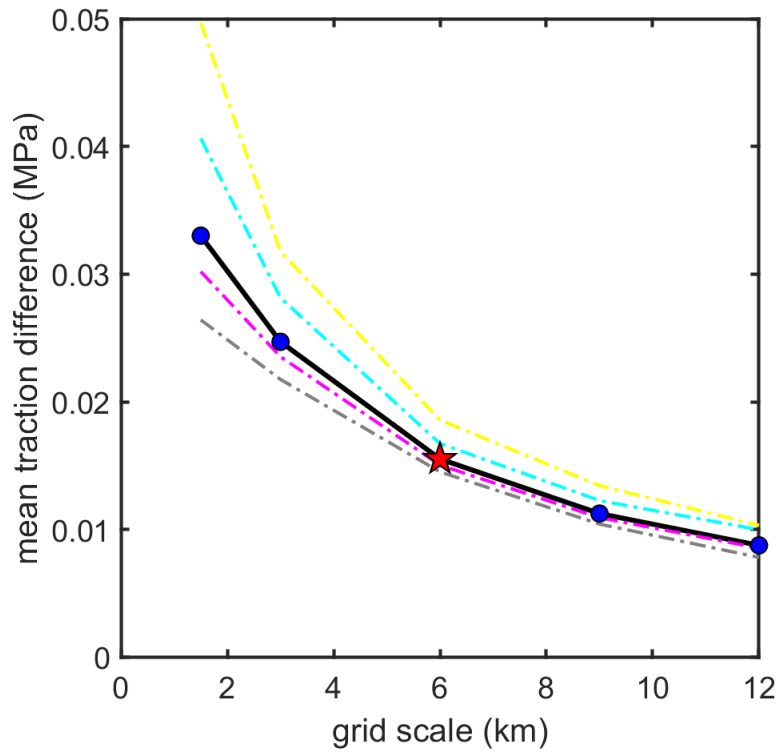
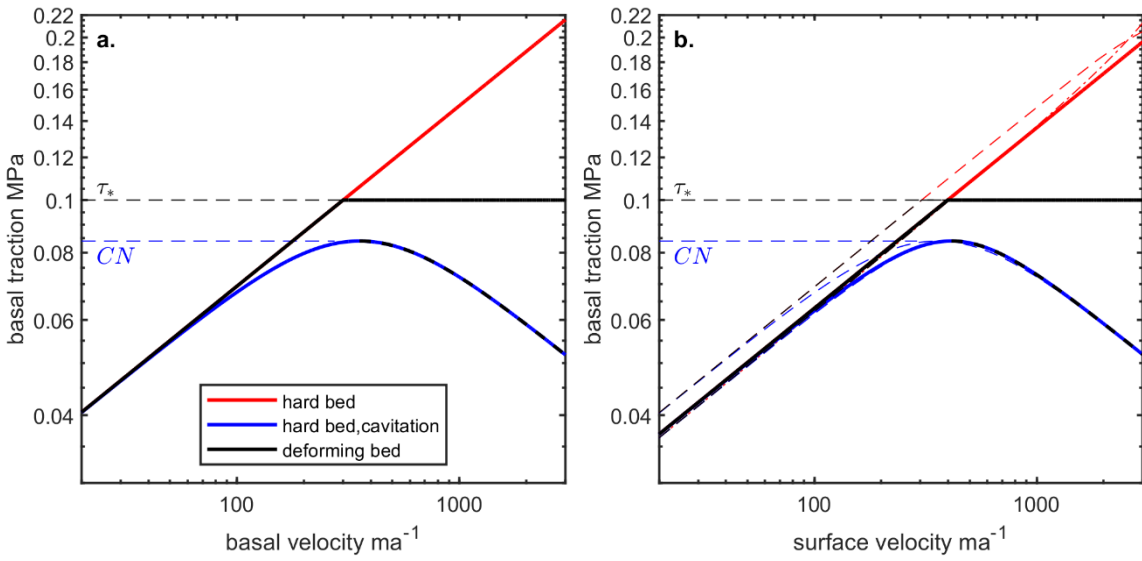


**Figure 1:** **a.** Multi-year surface velocity mosaic for GrIS (Joughin et al., 2018). **b.** Element nodes for the SSA (pink dots) and FS (black dots) inversions. The red contour shows the 100 m/yr velocity contour which delineates the regions from the stokes inversion used in the analysis **c.** Map of regions used in analysis. Black lines show drainage catchment delineation. The grey line indicates boundary of likely-thawed region. **d.** Driving stress calculated over 6 km x 6 km grid cells. **e.** Basal traction from SSA inversion averaged over 6 km x 6 km grid cells. **f.** Basal traction from FS inversion averaged over 6 km x 6 km grid cells.



535 **Figure 2:** Mean traction difference ( magnitude of SIA minus SSA) between the SIA and SSA approximation of basal traction as a function of grid scale. Decreasing deviation indicates the effect of higher-order stresses decreases with increasing grid length. Red star shows 6 km grid scale which is the primary grid scale used for our analysis. Dashed lines show same analysis for different subsets of the data (margin regions < 1200 m.a.s.l. – yellow line, interior regions > 1200 m.a.s.l. – grey line, thickness > 1500 m – magenta line, , thickness < 1500 m – cyan line).

540



545 **Figure 3: a.** Traction models that relate basal motion to basal traction for hard beds with and without cavitation and  
for deforming beds. *CN* indicates Iken's bound and  $\tau_*$  is the critical shear stress for deforming till (these parameters  
are set to fit the curves within the plotting space). **b.** The same relationships are shown with added deformation motion  
calculated with  $T = 0^\circ$  and  $H = 2500$  m. The bounds show deformation motion where parameters in the deformation  
calculation change with velocity. For the higher bound  $H$  is held constant at 2500 m while  $T$  increases from  $-25^\circ$  to  $0^\circ$   
550 through the velocity range. The lower bound,  $T$  is held constant at  $0^\circ$  and  $H$  decreases from 3000 m to 200 m through  
the velocity range.

555

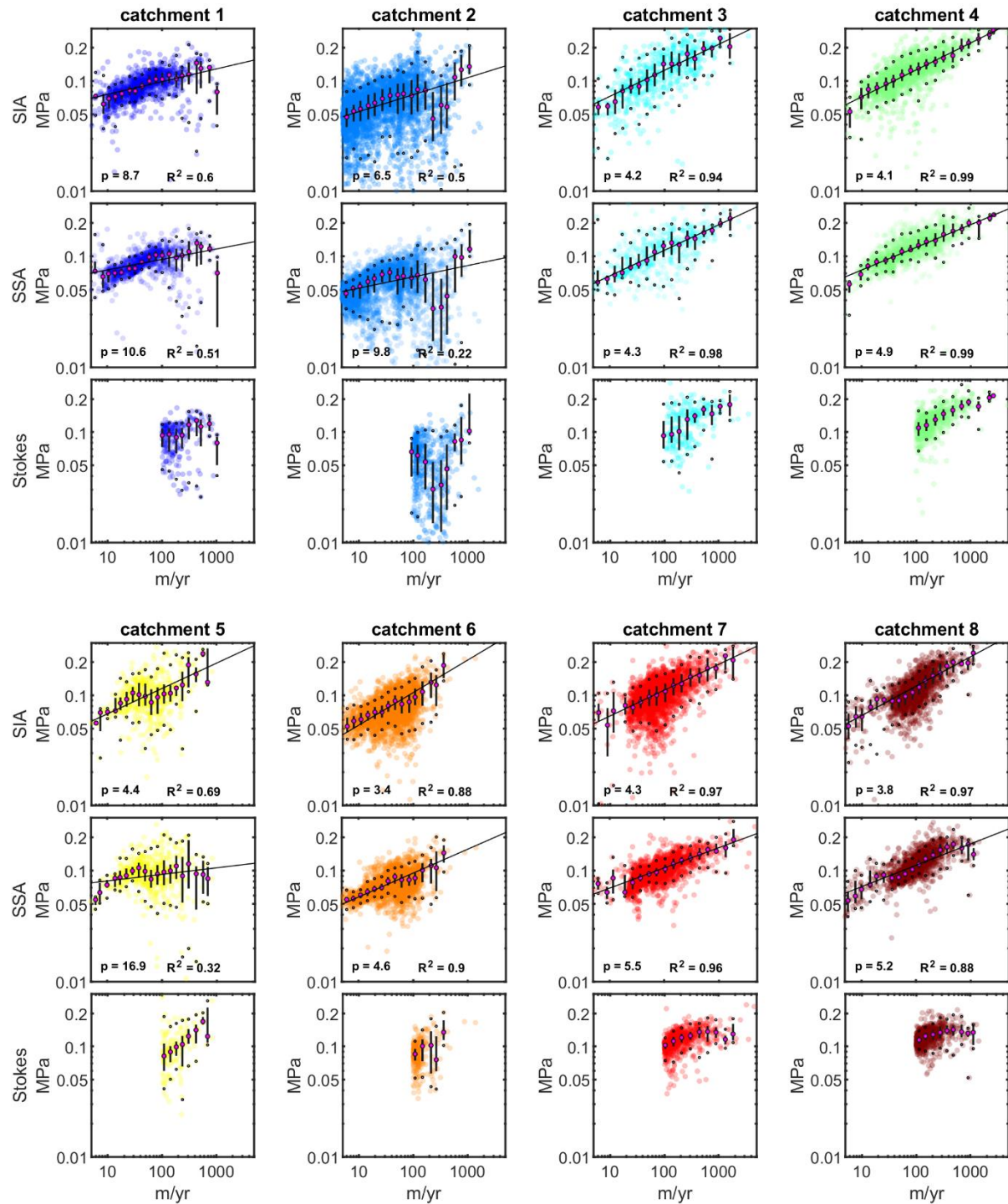
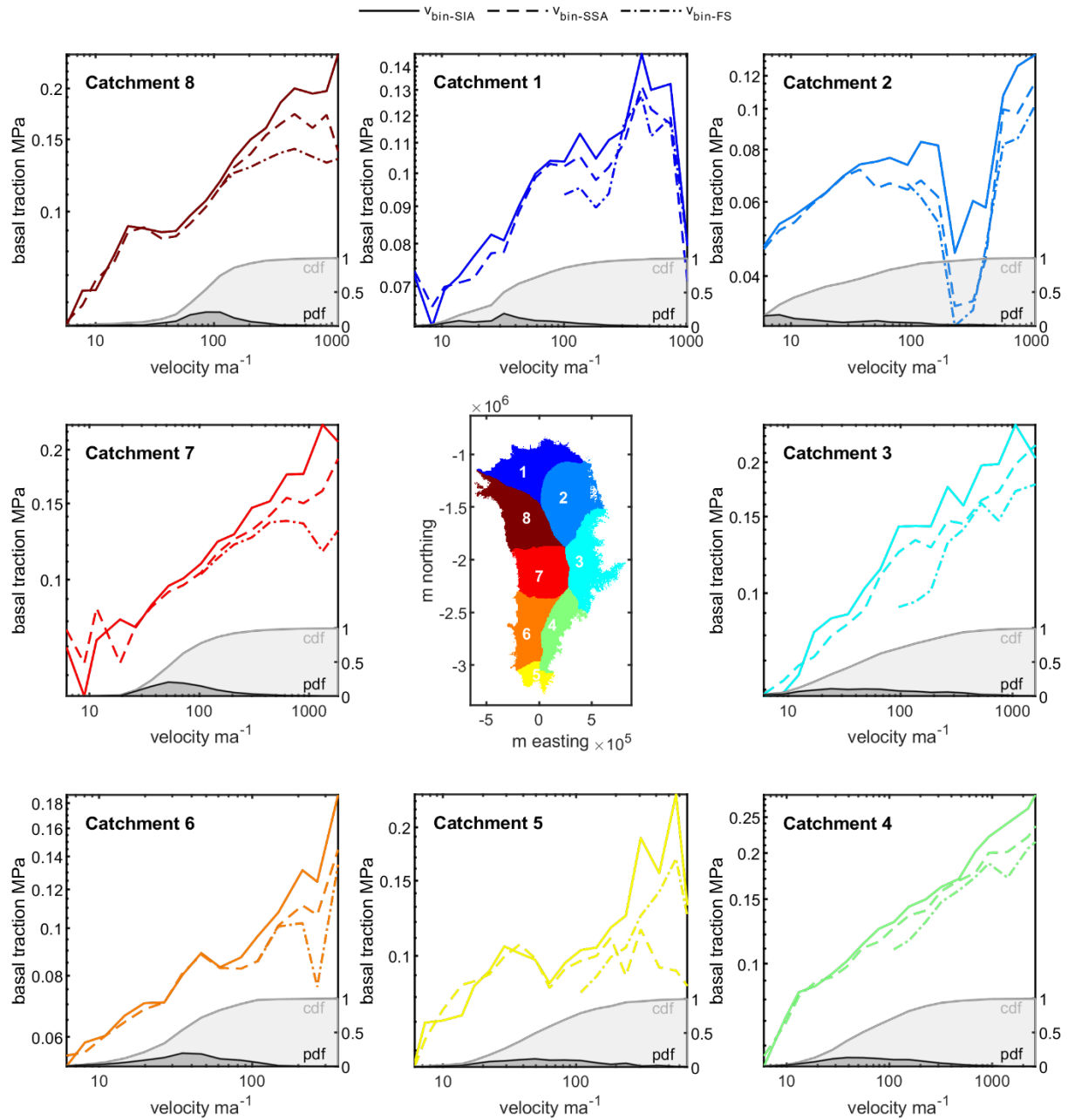


**Figure 4:** The velocity – traction relationship for the SIA, SSA, and Full Stokes inversions for all eight drainage catchments. Transparency is an indicator of data density, where opaque areas indicate four or more grid cells occupy the same marker area on the plot. Magenta markers show the median traction values for 20 logarithmically spaced velocity bins, the vertical bars show the interquartile range, and the black dots indicate the middle 90 percent of the

data. Black line shows a power law model fit to the binned data. No models were fit to the stokes relationships due to the velocity range ( $> 100$  m/yr) which is limited in our analysis.

565



570 **Figure 5:** The relationship between velocity and traction for the SIA (solid line), SSA (dashed line), and FS (dot-dash line) are shown together for each catchment. The right axis shows the probability density function (black line) and cumulative distribution function of the data (grey line) moving through the velocity range.

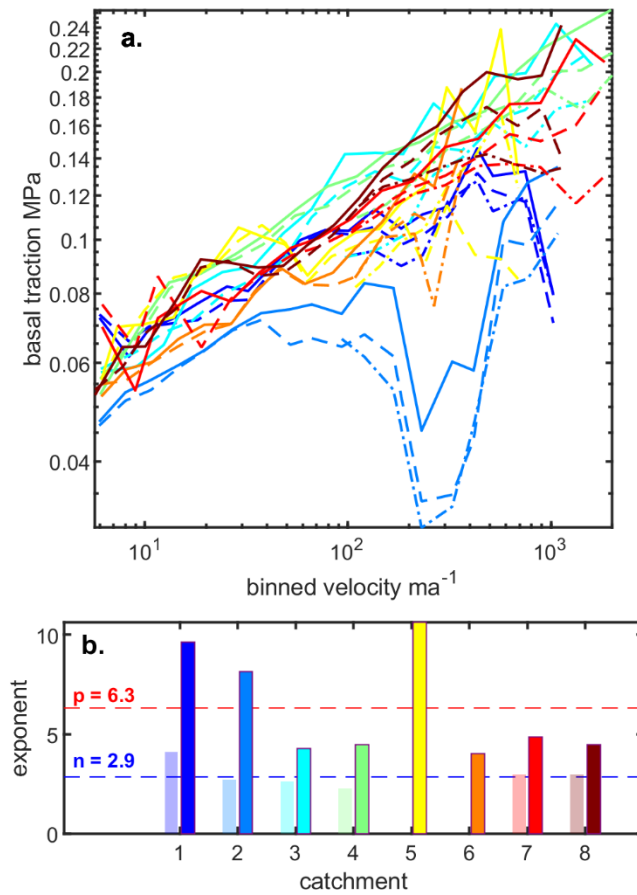
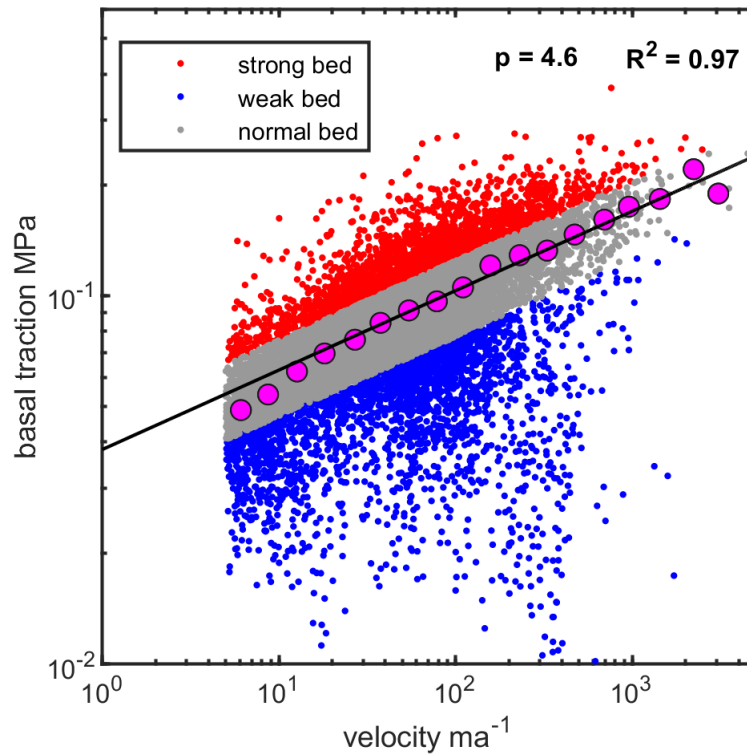


**Figure 6:** **a.** Binned velocity versus traction for all catchments and traction estimates (SIA – solid, SSA – dashed, FS – dash-dot). **b.**  $p$  for likely thawed regions (dark bars) and  $n$  for likely frozen regions (light bars) in each catchment. Values for each catchment are the average from the SIA and SSA. Dashed lines show the mean value for each exponent. No  $n$  is shown for catchment 5 and 6 which did not have enough grid cells to produce a reliable relationship (supporting Figure S5).



580

**Figure 7:** Weak and strong bed delineation is presented based on residuals from ice sheet-wide flow relationship. Ice sheet-wide flow relationship (black line) is calculated by averaging the SIA, SSA, and FS traction estimates for each grid cell in the likely thawed regions and fitting a power law model to the binned data. Pink markers show the binned velocity – traction relationship (median, 20 bins, logarithmically spaced). The residuals from the model relationship are used to delineate and map bed strength throughout Greenland. Strong and weak beds comprise the bottom and top 15% percent of the log-residual distribution, while grid cells with normal bed strength occupies the middle 70%.

585

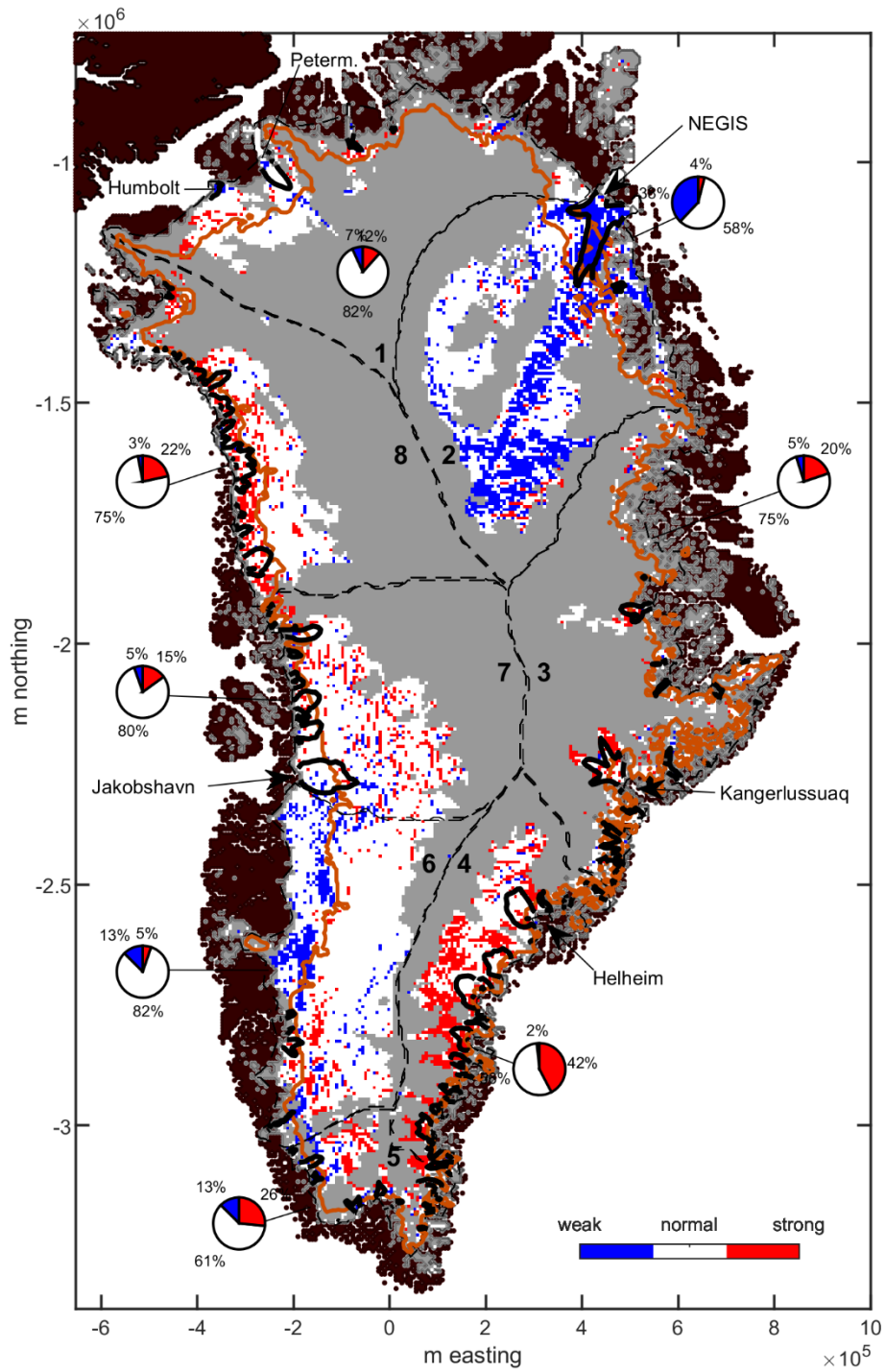


**Figure 8:** Map of weak and strong bed grid cells. Black contours separate fast and slow flowing regions of the ice sheet (200 m/yr contour). Orange line delineates the average snowline from 2001 to 2017 (Vandecrux et al., 2019).  
 590 Dashed lines delineate flow catchments. The small pie charts show the percentage of weak and strong regions within each catchment.

**Data and Code Availability:** All data used to generate this manuscript is currently archived and publicly available for download. Multi-year surface velocities: [doi.org/10.5067/QUA5Q9SVMSJG](https://doi.org/10.5067/QUA5Q9SVMSJG) Ice Surface Elevation: [doi.org/10.5067/H0KUYVF53Q8M](https://doi.org/10.5067/H0KUYVF53Q8M), Land/Ice classification: [doi.org/10.5067/B8X58MOBFUPA](https://doi.org/10.5067/B8X58MOBFUPA), Bed topography: [doi.org/10.5067/2CIX82HUV88Y](https://doi.org/10.5067/2CIX82HUV88Y), Basal thermal state map: [doi.org/10.5067/R4MWDWWUWQF9](https://doi.org/10.5067/R4MWDWWUWQF9), Snowline elevation: [doi:10.18739/A2V40JZ6C](https://doi.org/10.18739/A2V40JZ6C). Elmer/Ice code/output is available upon request.

**Acknowledgments:** This work was funded by the French National Research Agency grant ANR-17-CE01-0008.

**Author Contributions:** N.M. designed the study, analyzed the data, produced the figures, and is the primary author of the manuscript. F.G. contributed significantly to the data analysis and writing of the manuscript. F.G.-C. performed the basal traction inversions that were implemented with Elmer/ice and contributed to the writing of the manuscript. A.G. contributed to writing of the manuscript.

**Competing Interests:** The authors declare no competing interests.

## References

- Alley, R. B. and Joughin, I.: Modeling Ice-Sheet Flow, *Science*, 336(6081), 551–552, 2012.
- 605 Bons, P. D., Kleiner, T., Llorens, M., Prior, D. J., Sachau, T., Weikusat, I. and Jansen, D.: Greenland Ice Sheet: Higher nonlinearity of ice flow significantly reduces estimated basal motion, *Geophysical Research Letters*, 45(13), 6542–6548, 2018.
- Booth, A., Clark, R., Kulessa, B., Murray, T., Carter, J., Doyle, S. H. and Hubbard, A. L.: Thin-layer effects in glaciological seismic amplitude-versus-angle (AVA) analysis: implications for characterising a subglacial till unit, Russell Glacier, West Greenland, *Cryosphere*, 6, 909–922, 2012.
- 610 Bougamont, M., Christoffersen, P., A. L. H., Fitzpatrick, A. A., Doyle, S. H. and Carter, S. P.: Sensitive response of the Greenland Ice Sheet to surface melt drainage over a soft bed, *Nature Communications*, 5(1), 1–9, 2014.
- Carr, J. R., Vieli, A., Stokes, C., Jamieson, S., Palmer, S., Christoffersen, P., Dowdeswell, J., Nick, F., Blankenship, D. D. and Young, D. A.: Basal topographic controls on rapid retreat of Humboldt Glacier, northern Greenland, *Journal of Glaciology*, 61(225), 137–150, 2015.
- 615 Cavanagh, J., Lampkin, D. and Moon, T.: Seasonal variability in regional ice flow due to meltwater injection into the shear margins of Jakobshavn Isbræ, *Journal of Geophysical Research: Earth Surface*, 122(12), 2488–2505, 2017.
- 620 Christianson, K., Peters, L. E., Alley, R. B., Anandakrishnan, S., Jacobel, R. W., Riverman, K. L., Muto, A. and Keisling, B. A.: Dilatant till facilitates ice-stream flow in northeast Greenland, *Earth and Planetary Science Letters*, 401, 57–69, 2014.
- 625 Cooper, M. A., Jordan, T. M., Schroeder, D. M., Siegert, M. J., Williams, C. N. and Bamber, J. L.: Subglacial roughness of the Greenland Ice Sheet: relationship with contemporary ice velocity and geology, *The Cryosphere*, 13(11), 3093–3115, 2019.

- Csatho, B. M., Schenk, A. F., van der Veen, C. J., Babonis, G., Duncan, K., Rezvanbehbahani, S., Van Den Broeke, M. R., Simonsen, S. B., Nagarajan, S. and van Angelen, J. H.: Laser altimetry reveals complex pattern of Greenland Ice Sheet dynamics, *Proceedings of the National Academy of Sciences*, 111(52), 18478–18483, 2014.
- 630 Cuffey, K. M. and Paterson, W. S. B.: *The Physics of Glaciers*, Academic Press., 2010.
- Dahl-Jensen, D. and Gundestrup, N.: Constitutive properties of ice at Dye 3, Greenland, *International Association of Hydrological Sciences Publication*, 170, 31–43, 1987.
- Das, S. B., Joughin, I., Behn, M. D., Howat, I. M., King, M. A., Lizarralde, D. and Bhatia, M. P.: Fracture propagation to the base of the Greenland Ice Sheet during supraglacial lake drainage, *Science*, 320(5877), 778–781, 2008.
- 635 Dow, C. F., Hubbard, A., Booth, A. D., Doyle, S. H., Gusmeroli, A. and Kulesa, B.: Seismic evidence of mechanically weak sediments underlying Russell Glacier, West Greenland, *Annals of Glaciology*, 54(64), 135–141, 2013.
- Doyle, S. H., Hubbard, B., Christoffersen, P., Young, T. J., Hofstede, C., Bougamont, M., Box, J. and Hubbard, A.: Physical conditions of fast glacier flow: 1. Measurements from boreholes drilled to the bed of Store Glacier, West Greenland, *Journal of Geophysical Research: Earth Surface*, 123(2), 324–348, 2018.
- 640 Fahnstock, M., Abdalati, W., Joughin, I., Brozena, J. and Gogineni, P.: High geothermal heat flow, basal melt, and the origin of rapid ice flow in central Greenland, *Science*, 294(5550), 2338–2342, 2001.
- 645 Gagliardini, O., Cohen, D., Råback, P. and Zwinger, T.: Finite-element modeling of subglacial cavities and related friction law, *Journal of Geophysical Research: Earth Surface*, 112(F2), 2007.
- Gagliardini, O., Zwinger, T., Gillet-Chaulet, F., Durand, G., Favier, L., De Fleurian, B., Greve, R., Malinen, M., Martín, C. and Råback, P.: Capabilities and performance of Elmer/Ice, a new-generation ice sheet model, *Geoscientific Model Development*, 6(4), 1299–1318, 2013.
- 650 Gillet-Chaulet, F., Hindmarsh, R. C., Corr, H. F., King, E. C. and Jenkins, A.: In-situ quantification of ice rheology and direct measurement of the Raymond Effect at Summit, Greenland using a phase-sensitive radar, *Geophysical Research Letters*, 38(24), 2011.
- Gillet-Chaulet, F., Durand, G., Gagliardini, O., Mosbeux, C., Mouginot, J., Rémy, F. and Ritz, C.: Assimilation of surface velocities acquired between 1996 and 2010 to constrain the form of the basal friction law under Pine Island Glacier, *Geophysical Research Letters*, 43(19), 10–311, 2016.
- 655 Goelzer, H., Robinson, A., Seroussi, H. and van de Wal, R. S. W.: Recent Progress in Greenland Ice Sheet Modelling, *Curr Clim Change Rep*, 3(4), 291–302, 2017.
- Habermann, M., Truffer, M. and Maxwell, D.: Changing basal conditions during the speed-up of Jakobshavn Isbræ, Greenland., *Cryosphere*, 7(6), 2013.
- 660 Harper, J. T., Humphrey, N. F., Meierbachtol, T. W., Graly, J. A. and Fischer, U. H.: Borehole measurements indicate hard bed conditions, Kangerlussuaq sector, western Greenland Ice Sheet, *Journal of Geophysical Research: Earth Surface*, 122(9), 1605–1618, 2017.

- Harrington, J. A., Humphrey, N. F. and Harper, J. T.: Temperature distribution and thermal anomalies along a flowline of the Greenland ice sheet, *Annals of Glaciology*, 56(70), 98–104, 2015.
- 665 Hogg, A. E., Shepherd, A., Gourmelen, N. and Engdahl, M.: Grounding line migration from 1992 to 2011 on Petermann Glacier, north-west Greenland, *Journal of Glaciology*, 62(236), 1104–1114, 2016.
- Howat, I., Negrete, A. and Smith, B.: The Greenland Ice Mapping Project (GIMP) land classification and surface elevation data sets, *The Cryosphere*, 8(4), 1509–1518, 2014.
- 670 Howat, I., Negrete, A. and Smith, B.: MEaSURES Greenland Ice Mapping Project (GIMP) Digital Elevation Model from GeoEye and WorldView Imagery, Version 1., Boulder, Colorado USA. NASA National Snow and Ice Data Center Distributed Active Archive Center, doi:<https://doi.org/10.5067/H0KUYVF53Q8M>, 2017.
- Iken, A.: The Effect of the Subglacial Water Pressure on the Sliding Velocity of a Glacier in an Idealized Numerical Model, *Journal of Glaciology*, 27(97), 407–421, doi:10.3189/S0022143000011448, 1981.
- 675 Iverson, N. R., Hooyer, T. S. and Baker, R. W.: Ring-shear studies of till deformation: Coulomb-plastic behavior and distributed strain in glacier beds, *Journal of Glaciology*, 44(148), 634–642, 1998.
- Iverson, N. R., Cohen, D., Hooyer, T. S., Fischer, U. H., Jackson, M., Moore, P. L., Lappégard, G. and Kohler, J.: Effects of basal debris on glacier flow, *Science*, 301(5629), 81–84, 2003.
- 680 Joughin, I., MacAyeal, D. R. and Tulaczyk, S.: Basal shear stress of the Ross ice streams from control method inversions, *Journal of Geophysical Research: Solid Earth*, 109(B9), 2004.
- Joughin, I., Smith, B. E., Howat, I. M., Floricioiu, D., Alley, R. B., Truffer, M. and Fahnestock, M.: Seasonal to decadal scale variations in the surface velocity of Jakobshavn Isbrae, Greenland: Observation and model-based analysis, *Journal of Geophysical Research: Earth Surface*, 117(F2), 2012.
- 685 Joughin, I., Smith, B., Howat, I. and Scambos, T.: MEaSURES Multi-year Greenland Ice Sheet Velocity Mosaic, Version 1, Boulder, Colorado USA. NASA National Snow and Ice Data Center Distributed Active Archive Center, doi:<https://doi.org/10.5067/QUA5Q9SVMSJG>, 2016.
- Joughin, I., Smith, B. E. and Howat, I. M.: A complete map of Greenland ice velocity derived from satellite data collected over 20 years, *Journal of Glaciology*, 64(243), 1–11, 2018.
- 690 Joughin, I., Smith, B. E. and Schoof, C. G.: Regularized Coulomb friction laws for ice sheet sliding: application to Pine Island Glacier, Antarctica, *Geophysical research letters*, 46(9), 4764–4771, 2019.
- Kääb, A., Leinss, S., Gilbert, A., Bühler, Y., Gascoïn, S., Evans, S. G., Bartelt, P., Berthier, E., Brun, F. and Chao, W.-A.: Massive collapse of two glaciers in western Tibet in 2016 after surge-like instability, *Nature Geoscience*, 11(2), 114–120, 2018.
- 695 Kamb, B.: Rheological nonlinearity and flow instability in the deforming bed mechanism of ice stream motion, *Journal of Geophysical Research: Solid Earth*, 96(B10), 16585–16595, 1991.
- Kulesa, B., Hubbard, A. L., Booth, A. D., Bougamont, M., Dow, C. F., Doyle, S. H., Christoffersen, P., Lindbäck, K., Pettersson, R., Fitzpatrick, A. A. W. and Jones, G. A.: Seismic evidence for complex sedimentary control of Greenland Ice Sheet flow, *Science Advances*, 3(8), e1603071, 2017.

- 700 Kyrke-Smith, T. M., Gudmundsson, G. H. and Farrell, P. E.: Relevance of detail in basal topography for basal slipperiness inversions: a case study on Pine Island Glacier, Antarctica, *Frontiers in Earth Science*, 6, 33, 2018.
- Lampkin, D., Amador, N., Parizek, B., Farness, K. and Jezek, K.: Drainage from water-filled crevasses along the margins of Jakobshavn Isbræ: A potential catalyst for catchment expansion, *Journal of Geophysical Research: Earth Surface*, 118(2), 795–813, 2013.
- 705 Leeson, A., Shepherd, A., Briggs, K., Howat, I., Fettweis, X., Morlighem, M. and Rignot, E.: Supraglacial lakes on the Greenland ice sheet advance inland under warming climate, *Nature Climate Change*, 5(1), 51–55, 2015.
- Lindbäck, K. and Pettersson, R.: Spectral roughness and glacial erosion of a land-terminating section of the Greenland Ice Sheet, *Geomorphology*, 238, 149–159, 2015.
- 710 Lliboutry, L.: General Theory of Subglacial Cavitation and Sliding of Temperate Glaciers, *Journal of Glaciology*, 7(49), 21–58, 1968.
- Lüthi, M., Funk, M., Iken, A., Gogineni, S. and Truffer, M.: Mechanisms of fast flow in Jakobshavn Isbræ, West Greenland: Part III. Measurements of ice deformation, temperature and cross-borehole conductivity in boreholes to the bedrock, *Journal of Glaciology*, 48(162), 369–385, 2002.
- 715 Lüthi, M. P., Ryser, C., Andrews, L. C., Catania, G. A., Funk, M. and Hawley, R. L.: Heat sources within the Greenland Ice Sheet: dissipation, temperate paleo-ice and cryo-hydrologic warming, *The Cryosphere*, 2015.
- MacAyeal, D. R.: Large-scale ice flow over a viscous basal sediment: Theory and application to ice stream B, Antarctica, *Journal of Geophysical Research: Solid Earth*, 94(B4), 4071–4087, 1989.
- 720 MacGregor, J., Fahnestock, M. A., Catania, G. A., Aschwanden, A., Clow, G. D., Colgan, W. T., Gogineni, S. P., Morlighem, M., Nowicki, S. M. J., Paden, J. D., Price, S. F. and Seroussi, H.: A synthesis of the basal thermal state of the Greenland Ice Sheet, *Journal of Geophysical Research: Earth Surface*, 121(7), 1328–1350, 2016.
- 725 MacGregor, J., Fahnestock, M., Catania, G., Paden, J., Gogineni, P., Morlighem, M., Colgan, W., Nowicki, S. M., Clow, G., Aschwanden, A., Price, S. F. and Seroussi, H.: Likely Basal Thermal State of the Greenland Ice Sheet, Version 1, Boulder, Colorado USA. NASA National Snow and Ice Data Center Distributed Active Archive Center, doi:<https://doi.org/10.5067/R4MWDWWUWQF9>, 2017.
- Maier, N., Humphrey, N., Harper, J. and Meierbachtol, T.: Sliding dominates slow-flowing margin regions, Greenland Ice Sheet, *Science Advances*, 5(7), eaaw5406, 2019.
- 730 McCormack, F. S., Roberts, J. L., Jong, L. M., Young, D. A. and Beem, L. H.: A note on digital elevation model smoothing and driving stresses, *Polar Research*, 2019.
- Meierbachtol, T., Harper, J. and Johnson, J.: Force Balance along Isunnguata Sermia, West Greenland, *Front. Earth Sci.*, 4, 2016.
- 735 Minchew, B., Simons, M., Björnsson, H., Pálsson, F., Morlighem, M., Seroussi, H., Larour, E. and Hensley, S.: Plastic bed beneath Hofsjökull Ice Cap, central Iceland, and the sensitivity of ice flow to surface meltwater flux, *Journal of Glaciology*, 62(231), 147–158, 2016.

- Minchew, B., Meyer, C. R., Pegler, S. S., Lipovsky, B. P., Rempel, A. W., Gudmundsson, G. H. and Iverson, N. R.: Comment on “Friction at the bed does not control fast glacier flow,” *Science*, 363(6427), eaau6055, 2019.
- 740 Morland, L. and Johnson, I.: Steady motion of ice sheets, *Journal of Glaciology*, 25(92), 229–246, 1980.
- Morlighem, M.: IceBridge BedMachine Greenland, Version 3, Boulder, Colorado USA. NASA National Snow and Ice Data Center Distributed Active Archive Center, doi:<https://doi.org/10.5067/2CIX82HUV88Y>, 2018.
- 745 Morlighem, M., Rignot, E., Seroussi, H., Larour, E., Ben Dhia, H. and Aubry, D.: Spatial patterns of basal drag inferred using control methods from a full-Stokes and simpler models for Pine Island Glacier, West Antarctica, *Geophysical Research Letters*, 37(14), 2010.
- Morlighem, M., Williams, C. N., Rignot, E., An, L., Arndt, J. E., Bamber, J. L., Catania, G., Chauché, N., Dowdeswell, J. A. and Dorschel, B.: BedMachine v3: Complete bed topography and ocean bathymetry mapping of Greenland from multibeam echo sounding combined with mass conservation, *Geophysical Research Letters*, 44(21), 11–051, 2017.
- 750 Mougnot, J., Rignot, E., Bjørk, A. A., Van Den Broeke, M., Millan, R., Morlighem, M., Noël, B., Scheuchl, B. and Wood, M.: Forty-six years of Greenland Ice Sheet mass balance from 1972 to 2018, *Proceedings of the National Academy of Sciences*, 116(19), 9239–9244, 2019.
- 755 Poinar, K., Joughin, I., Das, S. B., Behn, M. D., Lenaerts, J. T. and Van Den Broeke, M. R.: Limits to future expansion of surface-melt-enhanced ice flow into the interior of western Greenland, *Geophysical Research Letters*, 42(6), 1800–1807, 2015.
- Rippin, D. M.: Bed roughness beneath the Greenland ice sheet, *Journal of Glaciology*, 59(216), 724–732, 2013.
- 760 Rogozhina, I., Petrunin, A. G., Vaughan, A. P., Steinberger, B., Johnson, J. V., Kaban, M. K., Calov, R., Rickers, F., Thomas, M. and Koulakov, I.: Melting at the base of the Greenland ice sheet explained by Iceland hotspot history, *Nature Geoscience*, 9(5), 366–369, 2016.
- Ryser, C., Lüthi, M. P., Andrews, L. C., Hoffman, M. J., Catania, G. A. and Hawley, R. L.: Sustained high basal motion of the Greenland ice sheet revealed by borehole deformation, *Journal of Glaciology*, 2014.
- 765 Schoof, C.: The effect of cavitation on glacier sliding, *Proceedings of the Royal Society A: Mathematical, Physical and Engineering Sciences*, 461(2055), 609–627, 2005.
- Seddik, H., Greve, R., Zwinger, T., Gillet-Chaulet, F. and Gagliardini, O.: Simulations of the Greenland ice sheet 100 years into the future with the full Stokes model Elmer/Ice, *Journal of Glaciology*, 58(209), 427–440, 2012.
- 770 Shapero, D. R., Joughin, I. R., Poinar, K., Morlighem, M. and Gillet-Chaulet, F.: Basal resistance for three of the largest Greenland outlet glaciers, *Journal of Geophysical Research: Earth Surface*, 121(1), 168–180, 2016.
- Smith, L. C., Chu, V. W., Yang, K., Gleason, C. J., Pitcher, L. H., Rennermalm, A. K., Legleiter, C. J., Behar, A. E., Overstreet, B. T., Moustafa, S. E., Tedesco, M., Forster, R. R., LeWinter, A. L., Finnegan,

- 775 D. C., Sheng, Y. and Balog, J.: Efficient meltwater drainage through supraglacial streams and rivers on the southwest Greenland ice sheet, *Proc Natl Acad Sci USA*, 112(4), 1001, doi:10.1073/pnas.1413024112, 2015.
- Stearns, L. A. and van der Veen, C. J.: Friction at the bed does not control fast glacier flow, *Science*, 361(6399), 273–277, 2018.
- 780 Stearns, L. A. and van der Veen, C.: Response to Comment on “Friction at the bed does not control fast glacier flow,” *Science*, 363(6427), eaau8375, 2019.
- Stevens, L. A., Behn, M. D., McGuire, J. J., Das, S. B., Joughin, I., Herring, T., Shean, D. E. and King, M. A.: Greenland supraglacial lake drainages triggered by hydrologically induced basal slip, *Nature*, 522(7554), 73–76, 2015.
- 785 Tulaczyk, S.: Ice sliding over weak, fine-grained tills: Dependence of ice-till interactions on till granulometry, *Glacial Processes, Past and Present*, 337, 159, 1999.
- Tulaczyk, S. M., Scherer, R. P. and Clark, C. D.: A ploughing model for the origin of weak tills beneath ice streams: a qualitative treatment, *Quaternary International*, 86(1), 59–70, 2001.
- Vandecrux, B., MacFerrin, M., Machguth, H., Colgan, W. T., As, D. van, Heilig, A., Stevens, C. M., Charalampidis, C., Fausto, R. S. and Morris, E. M.: Firn data compilation reveals widespread decrease of firn air content in western Greenland, *The Cryosphere*, 13(3), 845–859, 2019.
- 790 Walter, F., Chaput, J. and Lüthi, M. P.: Thick sediments beneath Greenland’s ablation zone and their potential role in future ice sheet dynamics, *Geology*, 42(6), 487–490, 2014.
- Weertman, J.: The Theory of Glacier Sliding, *Journal of Glaciology*, 5(39), 287–303, 1964.
- 795 Wright, P. J., Harper, J. T., Humphrey, N. F. and Meierbachtol, T. W.: Measured basal water pressure variability of the western Greenland Ice Sheet: Implications for hydraulic potential, *Journal of Geophysical Research: Earth Surface*, 121(6), 1134–1147, 2016.
- Zoet, L. K. and Iverson, N. R.: A slip law for glaciers on deformable beds, *Science*, 368(6486), 76–78, 2020.
- 800 Zwally, H. J., Giovinetto, M. B., Beckley, M. A. and Saba, J. L.: Antarctic and Greenland drainage systems, GSFC cryospheric sciences laboratory, Available at [icesat4.gsfc.nasa.gov/cryo\\_data/ant\\_grn\\_drainage\\_systems.php](https://icesat4.gsfc.nasa.gov/cryo_data/ant_grn_drainage_systems.php). Accessed March, 1, 2015, 2012.